Climate changes and human impact on the Mistras coastal barrier system (W Sardinia, Italy)

CLIMATE CHANGES AND HUMAN IMPACT ON THE MISTRAS COASTAL BARRIER SYSTEM (W SARDINIA, ITALY)

V. Pascucci[1], G. De Falco[2], C. Del Vais[3], I. Sanna[4], R.T. Melis[5], S. Andreucci[5]

[1] Università degli Studi di Sassari, Dipartimento di Architettura, Design, Urbanistica, Alghero, (Sassari), IT
Istituto di Geoscienze e Georisorse IGG-CNR (Pisa), IT
Institute of Geology and Petroleum Technologies, Kazan Federal University (Kazan) RU

[2] Istituto per l'Ambiente Marino IAMC-CNR, Torregrande (Oristano), IT

[3] Università degli Studi di Cagliari, Dipartimento di Storia, Beni Culturali e Territorio, Cagliari, IT

[4] Soprintendenza Archeologia, Belle Arti e Paesaggio per la città metropolitana di Cagliari e le province di Oristano e Sud Sardegna, Cagliari, IT

[5] Università degli Studi di Cagliari, Dipartimento di Scienze Chimiche e Geologiche, Cagliari, IT

Corresponding Author: Vincenzo Pascucci (pascucci@uniss.it)

Abstract

Integrated archaeological and geological studies conducted on Mistras coastal barrier system of central Sardinia showed that it developed as transgressive systems during the final stages of the Holocene sea level rise (final stage of the Holocene Climate Optimum, about 6300-6000 cal y BP), and become regressive (prograding) from about 2500 cal y BP, when sea level reached the present elevation.

The regression of the coast was, however, not continuous, but characterized by distinct Transgressive-Regressive phases (T-R), associated to precise climatic fluctuations, tied with global eustatic and climatic phases.

The first regression occurred between 2500 and 1900 cal y BP. This time interval, known as Roman Warm, coincides with the Phoenician, Punic and Roman attendance of the west Sardinia coast. At that time, areas close to the coastal cities had to host landings and perhaps ports probably located at short distance from the shoreline. Archaeological excavations and findings have documented that in the Mistras area Punic constructed a long boulder structure (probably dated from the 4^{th} Century BC) to better protect an incipient lagoon used as the harbour of the city of Tharros. This had the effect to modify the normal behaviour of the beach system that transformed from spit to barrier lagoon.

During the second regressive phase, the well-established beach lagoon system developed quasi continuously for more than 1200 years (650 and 1850 AD). This progradation started during a new warm period (Medieval) and continued favoured by gentle sea level fall occurred during the cold Little Ice Age time. During this time, after the abandonment of the city of Tharros and of the Sinis Peninsula, the Mistras area was poorly populated. As consequence, there was no more an active harbour and large sandy dunes developed and nourished the shore allowing a no man-influence progradation of the coast.

The third stage is the current one and begun about 165 years ago (post 1850 AD) after the relative sea level rise occurred after the end of the Little Ice Age.

Geological and archaeological data of western Sardinia barrier lagoon systems revealed that the Mistras barrier lagoon evolution was human influenced since the Punic time. The study pointed that little human activities on the coast could influence its natural behaviour and landscape, and that little climatic changes both positive and negative can induce progradation or erosion of the system as well.

Keywords: Holocene, Millennial scale transgressive-regressive cycles, Roman warm time, Tharros, Punic harbour, Sinis Penisula.

1. Introduction

Climate changes are one of the main actual topics, and to define how much the human impact has and is affecting them is of outmost importance. Investigating how environments could change in response to past climate changes is one of the keys to hypothesize possible future scenarios in the short/medium term.

The coastal areas are those where small eustatic and/or anthropogenic changes can cause significant environmental modifications (see for example Figure 5 of Mimura, 2013).

In this respect, studies of the Holocene sedimentary sequences of coastal plain and delta systems around the world have shown a similar depositional architecture dominated by a well-defined marine transgressive-regressive cycles, the so-called Holocene T-R cycles (Lowrie and Hamiter, 1995; Somoza et al., 1998; Amorosi et al., 2005; Amorosi et al., 2009; Boyer et al., 2005; Martin et al., 2007; Törnquist and Hijma, 2012; Tanabe et al., 2015; Milli et al., 2016). However, the direct link between the development of these Holocene short-term cycles and specific sea-level/climatic fluctuations is not so far, unequivocally proven (e.g. Amorosi et al., 2017 and reference therein).

The most complete, continuous and chronologically well-constrained set of millennial scale depositional cycles available for the Mediterranean basin is the sedimentary sequences of the Po plain subsurface (Italy; Amorosi et al., 2017). The reconstructed depositional cycles, called parasequences, represent episodes of rapid relative sea-level rise (T transgressive phase) followed by still stand condition (R regressive phase). The Authors recognize three (P1-3) Early Holocene parasequences recording alternating periods of rapid flooding and gradual shoaling. These are stacked in a retrogradational pattern that mostly reflect stepped, post-glacial eustatic rise. Conversely, the following five Middle to Late Holocene parasequences (P4-8) record a complex, pattern of coastal progradation and Po delta upbuilding that took place following sea-level stabilization during the highstand, starting at about 7000 years BP.

However, the Po river/delta system is nowadays, and was during the Holocene highstand, dominated by an extremely high sediment supply that may have masked the eustatic signal (Amorosi et al., 2005). Thus, an area with a relatively low sediment supply would potentially better record even very low amplitude eustatic/climatic changes occurred in the last 8-7000 y BP (Holocene highstand).

Costal barrier systems, consisting of elongated sandy barrier islands, spits, back-barrier basins (lagoon) and tidal inlets, are associated with the Holocene relative sea-level rise and still stand, sediment supply and local geological and physiographic inheritance (Davis and Clifton, 1987; Reinson, 1992; Weidman and Ebert, 1993; Fruergaard et al., 2015a). They are therefore useful environments to discriminate Holocene T-R cycles and if there has been or not a human interference on their natural evolution.

The Mistras coastal barrier system is nowadays, and is thought to be even during the Holocene, a low energy environment where riverine discharge is/was negligible (low sediment supply) and beaches are/were mainly fed by longshore currents carrying bioclastic-rich sand from the close and wide *Posidonia oceanica* sea grass meadows (Atzeni et al., 2007; De Falco et al., 2008).

Moreover, the Mistras coastal barrier system seems to be very sensitive even to minimal eustatic fluctuations. In particular, it has been hypothesised by Antonioli et al. (2017) that just 1 metre of absolute sea-level rise would modified the studied area from the present-day barrier-island lagoon system to an open bay. Thus, the Mistras system seems to be a very promising site where to study the millennia scale T-R cycles occurred during the last 8-7000 years BP. The Mid- to Late-Holocene period is regarded as being particularly relevant because the boundary conditions of the climate system have not changed substantially (in comparison with larger glacial–interglacial changes or with the beginning of the Holocene), and represents the period when an environment and climate comparable with the present was established (Wanner et al., 2008). However, in the Mediterranean basin the long history of human occupation and activities makes problematic to discriminate unequivocally between climate and non-climatic influences on the environment, especially during the mid to late Holocene (Zanchetta et al., 2012; Magny and Combourieu Nebout, 2013). Sardinia (Fig. 1A), in this context, is a key area for the definition of the interaction between human and climate occurred in the last 8-7000 years BP on landscape. The sparse population of the coast up to modern times is an advantage to distinguish the climate signal from the human induced modifications.

Integrated archaeological and geological studies have therefore conducted in the coastal barrier system of Mistras central Sardinia (Sinis Penisula) (Fig. 1B-D). In this site, human settlements are documented from the Middle Neolithic to the Iron Age (about 4900-730 BC, Depalmas and Melis, 2010; Usai, 2014), more intense during the Phoenician and Punic time (730-525 BC), and important during Punic (525-238 BC), Roman and Late Antique periods (238BC–476 AC) (Del Vais, 2014). During these last periods, the area was site of the important harbour/city of Tharros (Fig. 1C-D) (Acquaro et al., 1999; Spanu and Zucca, 2011).

Aims of this paper are: 1) to characterize the marine transgressive-regressive cycles that are recorded in the Mistras area since the last 8000 years and define the role of autocyclic vs allocyclic factors in controlling the stratigraphic architecture; 2) to compare the timing of the Mistras coastal dynamics with available eustatic curves for the Mediterranean Sea and the Red Sea basins; 3) to evaluate the role of external forcing (climate/human) on the control of the system dynamics.

2. Regional setting

2.1 The Mistras area

Mistras is located on the eastern part of the Sinis Peninsula on the north-western side of the Gulf of Oristano (Fig. 1C). The peninsula is a tombolo characterized by a promontory made of Miocene marlstones overlain by Pliocene basalts (Lecca et al., 1983; Carboni and Lecca, 1995). The promontory is connected mainland by Late Quaternary deposits, consisting of MIS5 sandy beachrock and MIS4 to MIS3 aeolianites (Forti and Orrù, 1995; Andreucci et al., 2009; Carboni et al., 2014). Presently, the western open seaside of the peninsula is draped by several pocket beaches, whereas the eastern is rockier and terminate with the Mistras coastal barrier system (Fig. 1C). The system is a barrier spit linked to the mainland, which partially closes the entrance of an elongated lagoon parallel to the shore (Fig. 1C) (Tigny et al., 2007). This barrier spit is a low energy beach system with the significant wave height from dominant winds very low (<1 m). Fetch is limited and low tidal range does not exceed 0.2 m (Ribotti et al., 2002). The foreshore sediments are medium-fine sands, whereas those of the shoreface/inner bay are fine to muddy sands extremely rich in sea grass leave fragments (Simeone and De Falco, 2012; De Falco et al., 2008). Riverine discharge is negligible and beaches are mainly fed by longshore currents carrying bioclastic-rich sand from the close and wide *Posidonia oceanica* sea grass meadows (De Falco et al., 2008). The minor amount of sand and gravel (pebbles) material derives from both cliff erosion and longshore currents (De Falco et al., 2003). Coastal dunes and/or aeolian sand sheets may locally develop.

2.2 Geology

Sardinia is one of the largest islands in the Mediterranean Sea (Fig. 1A). It represents a segment of the south-European plate that separated from the European as the result of an important rifting phase, which took place during the Oligocene–early Miocene (Cherchi and Montadert, 1982). Associated with the rifting, several NW–SE oriented basins formed (Carmignani et al., 2001). The easternmost is the Campidano graben (Fig. 1B). It contains more than 1000 m of Oligocene-Miocene syn rift deposits related to the opening of the western Balearic Basin, and 600 m of shallow-marine to continental Pliocene–Quaternary deposits related to opening of the eastern Tyrrhenian Sea (Fig. 1A) (Casula et al., 2001; Duncan et al., 2011).

Sardinia has been considered tectonically stable since the late Pliocene (Patacca et al., 1990; Gueguen et al., 1998). Within this generally stable setting, however, minor but consistent vertical movements at metre scale in local areas have been recognized (De Falco et al., 2015). A general subsidence occurred during the late Quaternary and allowed the deposition of marine to alluvial strata that crop out extensively all around the island. Commonly, the marine deposits consist of shallow-marine sandstones and conglomerates and are referred to the last interglacial-glacial stages (MIS5 to MIS1; Pascucci et al., 2014). The very low accommodation setting of Sardinia resulted, however, in a relatively thin Holocene succession (just 3-4 m thick), where continuous sedimentation along a single cross-section is very unlikely. The uppermost Holocene deposits (MIS1) are mostly represented by coastal barrier and/or coastal dunes cropping out along the coast of the island or as inland alluvial deposits (De Falco et al., 2015; Andreucci et al., 2017).

2.3 Sinis population

The Sinis area (Fig. 1C, D), as well as the whole Sardinia, was dominated by the Nuragic civilization in the most part of the 2nd millennium BC and beginning of the 1st millennium (about 3700-2730 y BP; Depalmas and Melis, 2010; Usai, 2014). At the end of the 8th century (or in the early 7th century) BC, the Phoenicians founded the city of Tharros at the southern end of the peninsula, in an area already populated during the Nuragic period; the main evidence of the Phoenician colony is represented by the necropolises and the Tophet, typical open air sanctuary or sacred burial area (Del Vais, 2014). During the second half of the 6th century BC, Tharros was conquered by the Carthaginians (Punic), who constructed several new buildings, including a monumental temple and the city defensive wall (Acquaro and Mezzolani, 1995). After the Roman conquest of Sardinia (238 BC), Tharros underwent to numerous transformations: i) the fortifications were renovated (2nd century BC), ii) a new urban system was established with the construction of roads using slabs of basalt, iii) numerous large and grand public buildings were constructed (2nd-3rd century AC). In the Late Antiquity and Early Middle Ages (5th-6th century AC; about 1600-1500 years BP) a gradual decline of the city of Tharros and the movement of the population inland occurred. Tharros and the Sinis area were completely abandoned in the Middle Ages due to the incursions of Saracens (Spanu, 1998).

3. Material and Methods

The Mistras coastal barrier system has been investigated with 11 continuous coring wells up to the maximum depth of 8 meters (Fig. 2 and supplementary material S1-S4).

Coring used a simple rotating core device with continuous pipes 1.5 m long. The depth control during coring was based on the number of pipes (or part of them). The compaction was evaluated comparing the length of the sampled core section, corresponding to the length of the pipe (1.5 m), with the length of the recovered core. Sediments were mainly sands and muddy sands, consequently the effect of compaction was < 30 cm. Deeper and sandy section were in some cases affected by fluidisation. In these cases, those sections were considered as a single unit. Cores were recovered in laboratory and described to define the main lithofacies in term of: sedimentary structures, however, poorly preserved, sediment texture, organic matter and carbonate contents, type and concentration of informative materials, including marine shells, plant fragments, and archaeological findings. Sediment samples were collected in correspondence to macroscopic changes in sedimentary features. A total of 82 samples were collected, sediments were dried at 60 °C, and sub-sampled by quartering for different analyses (see supplementary material S1-S3).

Grain size analysis was obtained by sieving and laser analysis. Sediments were carefully washed with distilled water and treated with H_2O_2 in order to remove organic matter. The sandy and muddy fractions were separated by wet sieving at 63 µm. The grain-size distribution was measured using dry sieving for the gravel/sand fraction and at half-phi intervals; the finer fraction (<63 µm) was analyzed using a Galai CIS 1 laser system.

The total organic matter was determined by “Loss on Ignition” (LOI) method, which measures the loss of dry weight after calcination at 500 °C for 3h. Carbonate content was determined using a Dietrich-Fruhling calcimeter. Note that, the “Loss on Ignition” is an estimate of the total organic matter contained in sediments (Dean, 1974). The Total Organic Carbon (TOC) is only a fraction of the total organic matter; that is, the weight of carbon contained in organic matter.

Multivariate statistic (factor analysis) analysis was used for the classification of sediment samples into sedimentary facies in order to distinguish sample groups both from compositional and granulometric characteristics. Factor analysis was applied to compositional and grain size data, previously transformed by the ranking method. A total of 82 cases and 9 variable were used (Fig. 3).

Twenty-two samples were collected along the cores for AMS ^{14}C radiocarbon dating performed at the laboratory of INNOVA SCaRL (University of Caserta, Italy). The samples were made by fibers of the seagrass *Posidonia oceanica* (11 samples), shells and bone fragments (3 and 2 samples respectively), wood fragments (2 samples) and seeds (3 samples). Because the production of atmospheric radiocarbon has varied through geological time, radiocarbon ages were calibrated to provide dates in calendar years before present (cal y BP). All samples were calibrated using CALIB 7.1 (Stuiver et al., 2017). In calibrating the samples we considered that the original depositional environment was a transitional zone influenced by both fluvial processes and marine water. Therefore for some dates a mixed IntCal13/Marine13 calibration method (Reimer et al., 2013) was applied according to what proposed by Di Rita et al. (2011) and Di Rita and Melis (2013). Local deviations of the marine reservoir effect were taken into account by using a ΔR value of 46 ± 40, which is the closest ΔR value (Bastia, Corsica), included in the Marine Reservoir Correction dataset (http://calib.org/marine; Stuiver et al., 2016) (Table 1).

Ground penetrating radar profiles (80-200-600 MHz antennas – IDS Industry system, Pisa, Italy) have been acquired perpendicular and orthogonal to the prograding beach ridges to better constrain their evolution (Fig. 2). However, the presence of a thick salt and muddy crust has not always allowed a good penetration of the electromagnetic waves.

Three archaeological excavations have been conducted: one underwater on April 2009 (A, Fig. 2) and two along the innermost beach ridge during summers 2014 and 2015 (B, C, Fig. 2). The archaeological research was aimed to determine the nature of the ancient attendance, known just for the presence of potsherds on the surface, and to verify if the area was the seat of an ancient harbour.

4. Results and interpretation

4.1 Sedimentary facies

The results of statistical analysis of the sediments collected along the core profile is reported in Fig. 3 and Table 2. Two factors were extracted accounting 75% of the total variance. Factor 1 (40% of the variance) was positively correlated to Fine fraction (Silt%, Clay%), organic matter % and sorting coefficient, and muddy organic sediments were separated from sandy sediments. Factor 2 (35% of the variance) is positively correlated to Gravel % and Coarse Sand % and inversely correlated to Medium-Fine sands, Mean Diameter and $CaCO_3$ content. Factor 2 separates gravelly and coarse sandy sediments from medium-fine sands (Fig. 3).

Facies analysis has allowed us to refer the Holocene drilled deposits to shoreface/inner bay, and foreshore and backshore (beachface) of sandy (and occasionally sand and gravel) beach environments (Davis and Duncan, 2004; Pascucci et al., 2009). In particular, the organic rich muddy sands to the shoreface/inner bay (not distinguishable due to the very shallow upper limit of the *Posidonia ocenaica* meadow, Tigny et al., 2007) and the sandy part to the beachface; that is, the gravelly coarse sands to the foreshore and the bioclastic medium-fine sand to the backshore (Table 2) (see also supplementary material S1-S4).

Archaeological findings were also used to distinguish sediments deposited underwater (shoreface), from those reworked in the swash zone (foreshore). Seeds, bones and wood fragments are better preserved to deterioration if deposited underwater. Foreshore deposits have been considered as sea level high stand markers (Goy et al., 2003; Nielsen and Clemmensen, 2009).

4.2 Archaeological results

The underwater investigation carried out on 2009 (A, Fig. 2) was aimed to define the long and straight submerged structure, oriented SW-NE (Del Vais et al., 2008, 2010). The structure is about 200 m long, 4 m wide and 1 m high, and occurs at depth of 0.40 m (were better preserved) from the surface of the lagoon (Fig. 4A-C). The structure is actually connecting the beach system with the small island located in the centre of the lagoon L2 (Fig. 4A-B).

The structure consists of two longitudinal walls made of well-squared, similar size (about 100 x 60 cm) but different thickness, blocks and slabs of sandstone arranged along two rows. The space between the two walls is filled with heterogeneous debris made of mixed mud and sand, levelled to form a horizontal plane (Fig. 4C). At intervals of 4/5 m, some blocks long up to 120 cm are placed orthogonal to the wall, with the short side facing outwards and the long embedded within the debris (Emplekton technique). This type of construction is normally realized to better resit to strong waves (Morhange et al., 2014).

On the southern side of the wall, an underwater excavation (UWE1, Fig. 4C) has identified numerous irregular boulders, at depth comprised between 0.40 and 0.80 m. Boulders are forming a continuous structure interpreted as breakwaters made to protect the wall from the open sea waves. Below the boulders, coniferous wood poles are vertically fixed on the floor at intervals of

0.50 m and assembled to other horizontal wood (leafy) (Fig. 4C). They are interpreted as structural elements made to contain the breakwater and to enhance the reinforcement of the main structure.

The archaeological excavation, conducted along the southern side of the wall, until the base of the structure and at depth of 1.10/1.20m, showed that coarse sand mixed with *Posidonia oceanica* balls (egagropili) and shells remains (*Cerithium* and *Cardium* genus) are present all along it. Fragments of Punic amphorae of cylindrical type, numerous grapevines, pinecones, pine nuts, nuts and hazelnuts were found as well.

Along the northern side of the wall a second underwater excavation (UWE2, Fig. 4C) highlighted that no boulders and only fine sand mixed with small scattered pebbles and rare shell remains are present.

Radiocarbon dating of three organic samples (C1-3, Table 1) collected at the base of the southern side of the wall (a pinecone flake and two fragments of the palisade woods, vertical and horizontal part, Fig. 4C) ranges from 2184±127, 2115±185, 1998±99 cal y BP (2311-1899 maximum and minimum cal y BP); that is, in the Roman Republican and Early Imperial periods. Ages are well correlated with the fragments of Punic transport amphorae discovered in the excavation and datable back to the 3rd-1st century BC. However, on a stratigraphic basis, it is possible to hypothesize that the wood palisade was placed in a later time than the construction of the wall, which is probably datable between 4th and 3rd Century BC (about 2350-2250 y BP).

The identified wall has precise comparison with other port buildings of Levantine origins, dating back to the 9th century BC, which extend to the successive periods, as in the case of the ports of Akko and Athlit in Israel (Del Vais et al., 2008; Morhange et al., 2014; Galili et al., 2007, 2010) and at the mouth of the Guadarranque River, in Spain (Bernal Casasola, 2010). Similar structures, documented in the Santa Gilla Lagoon (west of Cagliari, Fig. 1B) and interpreted as quays and docks, have been dated between the 5th and the 2nd century BC (Salvi, 1991, 2014; Soro and Sanna, in press). Moreover, sediments distribution demonstrates that the structure worked as a barrier against the marine action on its southern side, whereas it favoured the lagoon development on the northern one. Its construction, most probably, was necessary to enforce the natural protection offered by the open sea lagoon where boats anchored.

It is worthy to note that the wall during the first half of the 1800 AD was not submerged but used by the local fishermen (Del Vais et al., 2008); today, it is 40 cm underwater (mean sea level).

Archaeological underwater surveys have also documented the presence of a basaltic man made structure bounding the northern part of the Mistras system almost in the continuity with the wall investigated by underwater excavation (Fig. 4D). No data exist to date this structure.

The two archaeological excavations conducted along the innermost beach ridge on 2014 (B, coincident with the well S2, Figs 2, 5A) and 2015 (C; Figs 2, 5B) have allowed reconstructing the morphology of the Mistras system during 7th-3rd centuries BC (2630-2200 y BP) (Del Vais, 2015). The excavated strata are composed (from 1 to 2.3 m below the surface) of alternate of 3 to 10 cm thick silt to fine sand and organic rich layers (made of *Posidonia oceanica*) (Fig. 5A-B). Strata are horizontal in the lower part and slightly inclined toward the E of 1-2°over the top. They have been interpreted as shoreface deposits. The deposits from 0 to 1 m below the surface are composed of medium to coarse, well-sorted sand with sparse pebbles (rocks and pottery) and shell fragments more abundant in the uppermost part (Fig. 5A-D). Strata dip 5° toward the E. They have been interpreted as foreshore deposits.

The most common archaeological findings of the shoreface are seeds (mostly grapevines), remains of domestic animals (mostly sheep), worked and not worked woods, and well-washed pottery fragments (mostly transport amphorae). They range in age from the 7^{th} (6^{th} in the site C) to the 5^{th} century BC (4^{th} in the site C) (Fig. 2); that is, Phoenician and Punic time. Archaeological dates are confirmed by radiometric ages of seeds: 2537±172, 2529±170, 2528±170 cal y BP (2710-2365 maximum and minimum ages; Table 1).

The most common archaeological findings of the foreshore are pottery fragments (Fig. 5C). They range in age from the 5^{th} to the 3^{rd} Century BC (from the 4^{th} in the site C); that is, Punic time. Archaeological findings indicate the presence of an intensive trading area certainly connected to the city of Tharros since almost the 7^{th} Century BC.

4.3 Stratigraphy

Wells drilled in the Mistras area have encountered the pre-Holocene (Pleistocene) substrate at depth comprised between 3 and 5 meters. This is composed of bioclastic rich sandstone and claystone. The Holocene drilled sedimentary sequence have been grouped in five major transgressive-regressive cycles (**T1-T5**) approximately 2–4 m thick (Fig. 6). All but one of the bounding surfaces of these relatively thin units mark an abrupt landward facies shifting, and thus represent "sharp flooding surfaces". One, instead, simply testify a "deepening" trend, rather than an inland migration of the coastline (sensu Amorosi et al., 2005). These T-R cycles show an internal shallowing-upward trend possibly reflecting alternate episodes of rapid relative sea level rise and subsequent stillstand (Fig. 6). All but the first cycle has been dated using both archaeological and ^{14}C AMS age dating. The variability of ^{14}C data (2σ ranges) is reported in Table 1 and Figure 6. The 2σ intervals ranges between a minimum of 85 years and a maximum of 370 years. The T-R cycles developed for 3000 y (T1), 800 y (T2 and T3) and 500 y (T4). Consequently, the time intervals of the cycles are significantly higher than the larger variability of the obtained radiocarbon data.

The first cycle (**T1**) is 1.9 m thick and developed for at least 2000 years from about 7797±129 to 5878±116 cal y BP (7925-5762 minimum-maximum ages; Table 1) and has been drilled by the well S2 at depth between 1.8 and 4 meters below the present sea level (bpsl) and S7 between 6 and 8 m bpsl (see supplementary material S4).

Deposits of this cycle rest unconformable on Pleistocene substrate and are composed of organic and bioclastic rich mud passing upward to fine well-sorted sand. They are referred to the inner bay/shoreface to foreshore (beachface) (Fig. 6, see also supplementary materials S1 and S4). The estimated sedimentation rate was of about 1mm/y.

Interpretation

T1 represents the rapid sea level rise and coastline inland ingression (transgressive phase) followed by a clear shallowing upward facies pattern developed during the regressive (prograding) phase of the cycle. This phase is dominated by the first coastal barrier progradation system of the area related to the sea level stillstand occurred during the Holocene Climate Optimum (Rohling and De Rijk, 1999) (Fig. 7). No direct information are available defining the beach geometry associated to this cycle. The most probable feature, however, is a relative small cusp attached to the bedrock developing just north of the city of Tharros.

The second cycle (**T2**) is 2.1 m thick and developed for about 800 y, from about 2800 to 1998±99 cal y BP. Ages derive from both archaeological remains, dated back at the beginning of the Phoenician domination (2744 y BP) to the Roman Empire (1900 y BP) and ^{14}C ages (2884-1824 cal y BP, minimum-maximum ages). This second cycle has been closely investigated during the archaeological excavations (Fig. 5), drilled by S1, S2 and S10 wells (Fig. 6) and surveyed by GPR

(Fig. 8). T2 rests over a well-developed erosive surface, in few places associated with an erosive basal lag made of pottery and shell fragments (Fig. 6, and supplementary material S1 and S4). T2 is composed of alternation of medium to fine sand and organic rich layers in the lower part (shoreface) and medium to coarse well sorted sand and/or fine gravel in the upper one (foreshore) (Fig. 5). Strata dip 5° toward the E-ENE. Sedimentation rate was of 2.5 and 4 mm/y.

Interpretation

This second coastal barrier system developed primary as a cusp and evolved into a spit system (Clemmensen et al., 2001) linked to the mainland just north of the well S1 (Fig. 9). Spit prograded through time toward the E-ENE reaching about in the 4th Century BC (about 2350 y BP) the site of the first excavation (B, Fig. 2) and, in the 3rd Century BC (about 2250 y BP), the site of the second (C, Fig. 2, and Fig. 9). The well-marked unconformity separating cycle **T2** from **T1** indicates that between 6000 and 3000 y BP sea level dropped enough to expose and erode deposits of cycle **T1**. The measured minimum sea level fall was of 5 m bpsl (Fig. 6). Similarly to cycle **T1,** the inner bay/shoreface deposits overlaying the unconformity are associated with a rapid sea level rise and landward migration of the coastline occurred between 2884-2750 cal y BP. The following shallowing upward facies trend is, instead, interpreted as the result of a marine regressive phase occurred between 2710 and 2358 cal y BP (Fig. 6). This beach system progradation occurred during the Roman warm time high stand most probably until the 1900 y BP (Figs 6, 7, 9) (Roman Climatic Optimum of Perry and Hsu, 2000 and Van De Noor, 2013).

The third cycle (T3) is up to 4 m think and developed for about 800 y (maximum ages) from 1341±43 to 633±65 cal y BP (1384-568 minimum-maximum ages). It has been drilled by the south-easternmost wells (S3, S4, S5, S6) (Fig. 6 and supplementary materials S2 and S3). The lowermost part of **T3** is characterized by a transgressive lag made of sandstones and volcanic clasts gravel, coarse to very coarse sand, bones and pottery fragments. The middle part is composed of an alternation of fine to medium, poorly sorted sand and organic rich layer mostly made of *Posidonia oceanica* fragments (shoreface-inner bay). The upper part is made of fine to medium well-sorted sand (foreshore). The estimated sedimentation rate was very fast (5-6 mm/y) and the barrier prograded of 250 m in about 800 y.

Interpretation

The well-marked unconformity separating inner bay deposits of **T2** from the transgressive lag of **T3** cycle clearly indicates an abrupt sea level drop of about 4 metres occurred just after the Roman warm still stand (post 1900 cal y BP). The hiatus between the two cycles is of about 600 years (minimum age) and the erosive surfaces is well preserved in the all drilled wells (Fig. 6). The lower part of **T3**, made by transgressive lag and inner bay deposits (deepening upward facies trend), is interpreted as the result of a relatively fast sea level rise occurred between 1900 and 1300 cal y BP (minimum ages).

GPR profiles and wells correlation indicate that the third coastal barrier cycle prograded toward the E-ESE as barrier-lagoon system after 1341±41 cal y BP (Figs 8, 9). In this, time most probably the barrier lagoon L2 system formed as an isolated barred feature. Progradation continued toward the ESE for the entire cycle (Fig. 6).

The fourth cycle (**T4**) is up to 2 m thick, developed for about 500 y (maximum ages) and span from 631±62 cal y BP to 200 y BP (693÷200 minimum-maximum ages). The age of 200 y BP is derived from chronicle of the 1800 AD indicating that the Punic-Roman wall, at that time, was not submerged (Del Vais, 2008). T4 has been drilled by wells S4 and S5 and is characterized in the lower part by mud bearing *Posidonia oceanica* fragments alternated with fine sand (inner bay/shoreface). The upper part is composed of medium to fine grained bioclastic rich sand (foreshore-backshore) (Fig. 6 and supplementary material S3).

Interpretation

A short very fast sea level fluctuation (fall and rise), not higher than 1 meter, is thought have occurred around 631±62 cal y BP. This fluctuation is documented by the alternation foreshore-shoreface-foreshore recognized in the uppermost part of the wells S4-S5 (Fig. 6 and supplementary material S3). Beach ridges of **T4** cycle developed at a relative low elevation than the previous (Figs 6, 9B). This is interpreted as a general continuous moderate (max 1 m in total, most probably 0.5 m) sea level fall occurred from 568-630 cal y BP and 165 y BP that allowed the barrier lagoon system prograding toward E-ESE (Figs 6, 9).

The fifth cycle (**T5**) is associated to 25 m wide, modern narrow beach bounding the L3 lagoon. Bioclastic-rich, medium to fine sized sand are the most common sediments. Coppice dunes are forming in the backshore where sand thickness does not exceed 1 m. Aerial photos show that the beach is a growing toward ENE as spit system (Fig. 9).

Interpretation

Similarly to cycle **T4**, the inner bay/shoreface deposits of **T5** are associated with a post 165 y BP (1850 AD) short and very fast sea level fluctuation (fall and rise). As consequence of the sea level rise of about 30-40 cm, the barrier system reached the present day level and slightly prograded seaward. The reduced sediment supply allowed the long shore currents being the dominate factor in controlling the beach progradation.

5. Discussion

5.1 Coastal barrier evolution

It is widely accepted that as soon as the Holocene sea level rise decreased coastal barrier developed (Fruergaard et al, 2015b; Longhitano et al., 2016; Vink et al., 2007). According to the scheme proposed by Lambeck et al. (2011) the rate of the post Last Glacial Maximum (LGM) sea level rise decreased at about 6800 cal y BP when it was between 10 and 4.5 metres below the present sea level (bpsl) (Fleming et al., 1998; Sivan et al., 2001; Galili et al., 2005; Antonioli et al., 2015). The Holocene reached its climate optimum around 6500-6200 cal y BP and mean temperature was just little higher (1-2 °C, Stranne at al., 2014) or similar to the today one (; Davis et al., 2003) (**P** of Perry and Hsu, 2000; Fig. 6). Between 6300 and 5900 cal y BP, the Mistras area experienced the first evidence of coastal barrier formation soon after an important transgressive phase. This barrier formed when the sea level was 2-2.5- m bpsl (Fig. 6). This implies that during the Holocene optimum sea level was at least about 2 m lower than the present (Fig. 7). This is in good agreement with the proposed Holocene sea level rise curve of the Mediterranen Sea (Lambeck et al., 2004, 2011; Zazo et al., 2008), with the archaeological observations made by Sivan et al. (2001) along the coast of Israel, and with the curve proposed for the Red Sea by Grant et al. (2012). It is, instead, slightly higher respect the values of -8 m of the global curve by Perry and Hsu (2000) (Fig. 7).

No archaeological findings relative to this time interval have been found in the Mistras area confirming that there was not intense land and coastal use of area until at least the Final Neolithic (3500 BC, Pittau et al., 2012; Di Rita and Melis, 2013). However, it is worthy to note that Pittau et al. (2012) indicated that a Neolithic site in southern side of the Oristano Gulf was abandoned between 7400-7030 cal y BP. This may suggest that Neolithic sites although present in the areas where abandoned before the beginning of T1 deposition, possibly as consequence of important landscape changes related to sea-level rise.

A time gap of about 3000 years separates the first cycle from the second. None of the drilled wells encountered deposits dated between 6000-3000 cal y BP (Fig. 6). An abrupt sea level drop of 5 m (minimum; Figs 6, 7) possibly occurred between 6000 to 3000 cal y BP, allowed an important erosion of **T1**-cycle deposits. During this forced regressive phase the coastline shifted seaward of more than a kilometre and a system of marshes, ponds with ephemeral fluvial systems developed on the newly formed coastal plain. Sandy-mud deposits referred to a lagoon with marine and fluvial influence dated at 4228±40 cal y BP and fluvial deposits dated at 5647±63 and 2744±205 cal y BP recognized respectively in the close MR1 well (Fig. 2) (Di Rita and Melis, 2013) and Tirso river coastal plain (Oristano, Fig. 1B) (Melis et al., 2017) may confirm this hypothesis.

At about 3000 cal y BP, the studied wells record the evidence of a rapid sea level rise (20 mm/y). Sea reached the present day level about 500 years later allowing the developing of the **T2** spit beach system (Fig. 6). The spit prograded from about 2500 until 1900 cal y BP at the rate of 0.4 cm/y. This fast spit growing delimited on its northern side a sheltered lagoon (L2, Fig. 9). Archaeological excavations did not identify harbour infrastructures of Phoenician period (8^{th}-6^{th} centuries BC – about 2744-2545 y BP) and thus, we can hypothesize that in this time boats where mostly anchored in front of the spit beach. As the spit prograded toward the ENE, boats anchorage moved on the same way, as documented by the archaeological findings becoming younger toward the ENE.

Probably around the 4^{th} Century BC (2400-2300 y BP) the presence of a sheltered lagoon with some small-scattered islands would have induced the Punics of Tharros to build structures connecting the spit with the islands, to better protect the lagoon from sea storm (or enemies), and use it as harbour. From that 4th Century BC the sandstone blocks and also the basalt boulder structures (Fig. 4) become artificial barriers protecting the lagoon from the open sea (Fig. 9). However, the barriers acted also as preferential accumulation place of the sand carried by the small rivers feeding the lagoon and by longshore NE oriented current.

The lagoon water depth during the Punic time was deeper than today and a perfect-safe place where to anchor the boats. This natural favourable situation was also used by the Romans (Republican Roman time 2nd-1st Century BC) who continued using the Punic wall, also reinforcing it with wood palisade, as dock of the natural harbour. During the Imperial Roman time (since 2000 y BP), however, the lagoon most probably become shallower and hardly connected with the open sea because of the sand accumulation and the relative sea level fall. It was therefore abandoned and the new harbour was moved more seaward where the sea level was high enough to avoid boat shoaling (Roman imperial period; Acquaro et al., 1999).

Between 1998±99 and 1341±43 cal y BP a new sea level fall of about 4 metres occurred, the spit system deactivated and the coastal barrier system migrated seaward reaching most probably the position of the well S5 (Fig. 9).

A relatively rapid marine transgression, marked by a well-developed basal lag, occurred at about 1341±43 cal y BP. At its end, sea level reached again the present high level. This phase of sea level fluctuation is not described in any of the Mediterranean Holocene sea level curve models (i.e. Lambeck et al., 2011; Antonioli et al., 2015; Vacchi et al., 2016).

The still stand occurred just after 1400 cal y BP at Mistras site allowed the progradation of the beach system **T3** (Figs 6, 9). The first beach ridges of this new system formed between S2 and S1 wells; that is, slightly seaward than the previous (Figs 6, 9). This new progradation, however, was strongly influenced by the presence of the structures made during Punic times. Thanks to these, the coastal barrier system developed attached to them and prograded toward the ESE; that is, perpendicular to the previously naturally evolved spit system. Landward a protected back barrier lagoon (L2) formed. The beach system prograded more or less continuously for about 800 years until 1380 AD (633±65 cal y BP) (Fig. 6) when a fast sea level fluctuation, placed at 631±62 cal y BP is recorded. This fluctuation occurred almost at the beginning of the Little Ice Age (LIA, 1250-1860 AD) (Le Roy Ladurie, 1959; Fagan, 2000) and is marked by less than a metre sea level drop (probably just 50 cm). A relatively moderate sea level fall continued during the entire LIA cold phase allowing the beach ridge system progradation until 1750-1850 AD. We do not have any precise time constraining for the end of cycle **T4**. However, chronicles of the 1800 AD (Del Vais et al., 2008) indicate that the Punic wall was visible and used as short cut by local fishermen. This implies that sea level was probably 50 cm below the present. At the end of 19th century (post 1850 AD) sea level rose again reaching the present day level and beaches newly prograded (**T5** cycle). Today, they are mostly fed by a longshore current generating a new spit system (Fig. 9).

5.2 Climate and human occupation

During the last ca. 5000–6000 years BP the climate did not substantially varied in comparison with larger glacial–interglacial changes or with the beginning of the Holocene (Wanner et al., 2008). Consequently, sea level was more or less stable (Fig. 7) allowing the establishment of important coastal urban centres (Galili et al., 2005). Inside this general climate stability, however, relatively small climate changes occurred generating remarkable environmental changes, such as coastal retreat or advance, river mouth migration, etc. (Zazo et al., 2008; Melis et al., 2017). People have always tented to modify the environment to contrast these changes building walls, groins, palisades, etc. However, in densely populated area, like the Mediterranean basin, the long history of human occupation and activities makes problematic to unequivocally discriminate between climate and non-climatic influences on the environment, especially during the last 3000 years (e.g. Roberts et al., 2001, 2011; Zanchetta et al., 2012; Magny and Combourieu Nebout, 2013).

During the Holocene optimum warm time (about 7000-6000 cal y BP, **P**, Fig. 7; Rohling and De Rijk, 1999; Perry and Hsu, 2001; Davies et al., 2003) the Mistras coastal barrier systems developed. It is worthy to note that beach regression begun at about 6300 cal y BP (Fig. 6); that is, during the receding phase of this warming time (Fig. 7).

The about 3000 years long hiatus found in the well S2 documents that an important environmental change occurred during this time span. This can be correlated with the cold phases known as “Sahara Aridity” or the Post Late Neolithic arid phase (Walsh, 2014), Piora Oscillation (Baroni and Orombelli, 1996) or to the Bond n. 4 event (Bond et al., 2001) during which the coldest period after the Young Dryas occurred (**J-K**, Fig. 7) (Perry and Hsu, 2000). This Oscillation marks the end of the Atlantic climate regime, and the beginning of the Sub-Boreal (Blytt-Sernander Sequence, Rydin and Jeglum, 2013). During this relatively cold time, the Mistras area (and the all Sardinia as well as) was scarcely populated.

Climate amelioration begun around 4000 cal y BP (**R**, Fig. 7) and in Sardinia the Nuragic Civilization developed. This climatic change allowed a more intensive grazing and breeding with, as main consequence, important landscape modifications (Depalmas and Melis, 2010). Sea level rose up to the present level reaching the highstand about 2500 cal y BP. Climatically, the period from 2500-1800 cal y BP is considered the Roman Optimum (**S** of Fig. 7) during which the exceptional climate stability and favourable conditions also coincides with the rise of Roman Empire (Mensing et al., 2015). During this time, the Mistras/Tharros area experienced warm climate conditions that favoured not only the development of one of the most important Phoenician-Punic-Roman cities of Sardinia but also the agriculture and animal breeding. The land close to the city was pastured and cultivated with the introduction of important economic plants such as *Vitis*, *Olea* and *Quercus suber* (Di Rita and Melis, 2013; Del Vais, 2014).

The Roman warm time was followed by a relative cold period (**M**, Fig. 7) during which some of the biggest Migration of Nation occurred (Perry and Hsu, 2000). This time interval in the Mistras area lasted for about 400 years (1800 to 1400 cal y BP) and both the city of Tharros and the surrounding areas were abandoned.

The following Medieval Warm Period (MWP) is placed between 1500-1000 cal y BP (500 to 1000 AD) (Mensing et al., 2015). Temperatures in the northern hemisphere began warming after 500 AD and reached the maximum between 850 and 950 AD (**T** of Fig. 7) and a maximum temperature anomaly of 0.6° C (Christiansen and Ljungqvist, 2012). During this warm time, the Mistras/Tharros area was poorly populated and the low human pressure on the coastal system and the relative sea level high stand allowed the wide progradation of the barrier system (Fig. 9).

There is no consensus on when the Little Ice Age started (**N**, Fig. 7) and ended, but the Medieval warming period ended around the year 1300 AD (Esper et al., 2002). The beginning of this new cooling time had as first pick the Wolf Minimum (1280-1350 AD) followed by the Spörer (1450–1540 AD), the Maunder (1645-1715 AD) and by the less marked the Dalton (1790–1820 AD). During the Little Ice Age winters were alternately mild and very cold just like today, but generally the climate was colder than today with a very cold pick around 1690 AD. This is normally considered the culmination of the Little Ice Age. After the winter of 1850 AD, also very cold, the modern warm period began (Büntgen et al., 2011; Christiansen and Ljungqvist, 2012; McCormick et al., 2012). The Mistras/Tharros area was still scarcely populated and the gentle sea level drop favoured the progradation of the wide coastal barrier system (**T4**) (Figs 6, 9). It is worthy to note that a climatic fluctuation is recorded around 1384±62 AD (631±62 cal y BP). This is coincided with the short interstadial Wolf- Spörer that for some reasons is apparently well recorded in the Mistras area.

The Modern warming Period begun around 1850 AD (**U**, Fig. 7). The scarce sediment supply from inland had as consequence that the modern progradation (**T5**) is mostly due to long-shore current responsible of the reforming of a spit system.

5.3 Linking T-R cycles to eustatic/climate changes

Since the pioneer work of Lowrie and Hamiter (1995) an increasing literature reports the occurrence of millennial to sub-millennial scale depositional cycles dominated by an abrupt landward/seaward shifting of the shoreline within the Holocene T-R cycle (ca. 12000-0 y BP). However the autocyclic and/or allocyclic nature of these low-rank cycles is matter of debate (e.g. Amorosi et al., 2017 and reference therein).

In order to discriminate the allocyclic and/or autocyclic nature of the 5 T-R observed at Mistras area, they have been tentatively linked with the available Holocene eustatic curves for the Mediterranean basin and the Red Sea (Morhange et al., 2001; Zazo et al., 2008; Lambeck et al., 2011; Grant et al., 2012; Antonioli et al., 2015; Vacchi et al., 2016) along with the millenial-scale climate changes based on the solar insolation output (Perry and Hsu, 2000) and the cold "Bond" events (Bond et al., 1997, 2001; Zazo et al., 2008). In particular, we have focussed our attention on the origin of the surface at the base of each T-R cycles. If a basal surface can be tied in age with eustatic and/or warming peaks, is therefore considered driven by allocyclic factors and of regional to supraregional importance.

The base of **T1** cycle dated at about 7800 cal y BP is well tuned with the sea level peak from Mediterranean basin (Antonioli et al., 2015; Zazo et al., 2008) and Red Sea curves (Grant et al., 2012) as well as with the warming phase **P** of Perry and Hsu (2000). Moreover, in several Italian coastal plains facing both the Tyrrhenian Sea and the Adriatic Sea the age of the maximum flooding surfaces is placed between 8500 to 7000 cal y BP in good agreement with **T1** cycle (Amorosi et al., 2017; Milli et al., 2016 and reference therein). Thus, the flooding surface at the base of **T1** cycle seems to be controlled by eustatic and climatic factors (allocyclic nature) and represents a true flooding surface (shoreline inland migration).

The base of **T2** cycle dated at about 2800 cal y BP cannot be tied with the Mediterranean related sea level curve (Lambeck et al., 2004, 2011; Antonioli et al., 2015; Vacchi et al., 2016) but can be associated with the transgressive phase recoded in Almeria (Spain, H4 Unit of Goy et al., 2003; Zazo et al., 2008) and in the Red Sea (Grant et al., 2012) and tuned with the warming phase **S** (Roman warm) of Perry and Hsu (2000) (Fig. 7).

The age of the base of **T2** cycle (older than 2817±67 cal y BP), although slightly older than the base of parasequence P6 (ca. 2600 cal y BP; Amorosi et al., 2017) and of the second phase of Tiber delta progradation system (ca. 2700 cal y BP; Milli et al., 2016), seems to be controlled by eustatic and climatic factors (allocyclic nature). The **T2** cycle flooding surface represents a true shoreline inland migration occurred during the Warm Roman time. It is worthy to note that at Mistras site the maximum inland marine Holocene ingression occurred at 2574±141 cal y BP (Fig. 7).

The base of **T3** cycle is placed around 1341±43 cal y BP and cannot be tied with the Mediterranean related sea level curve (Antonioli et al., 2015), only partially with H5 Unit of Almeria (Zazo et al., 2008) and with the post 1000 cal y BP transgressive phase recorded in the Red Sea sequence (Grant et al., 2012). However, this transgressive phase is in relatively good agreement with the warming **T** phase (ca. 1500 cal y BP) of Perry and Hsu (2000) and could be associated with the so-called Medieval Warm Period (MWP 1065-765 cal y BP; Mensing et al., 2015). The **T3** cycle almost match the age of parasequence P7 (1500 cal y BP) of Amorosi et al. (2017). Moreover the reconstructed phase of sea level drop of at least 4 m minimum at about 1900-1500 cal y BP well fit with the cold "Bond event 1" (1400 cal y BP). Thus, **T3** cycle seems to be mainly controlled by climatic factors (allocyclic nature) and the flooding surface may represents a true shoreline inland migration. However, there is the need to verify these data in other areas to fully prove this rapid eustatic fluctuation.

The base of **T4** cycle cannot be fitted with any peaks from Mediterranean basin and Red Sea eustatic curves (Antonioli et al., 2015; Grant et al., 2012) and with any warming phase. The climate curve shows a general cooling trend with a cold peak place at 670 cal y BP (Wolf Minimum). The base of **T4** cycle (631±62 cal y BP) is in broadly agreement with parasequence P8 (post 800 cal y BP) observed in the subsurface of the Po plain (Amorosi et al., 2017) and with H6 Unit of Almeria (Goy et al., 2003). Thus, this surface could simply be the evidence of a "deepening" (sensu Amorosi et al., 2005) mainly controlled by autocyclic factors with no significant “true” sea level rise.

The base of **T5** cycle (presumably at 1860 AD) cannot be fitted with any sea level peaks from Mediterranean basin and Red Sea curves (Antonioli et al., 2015; Grant et al., 2012) but is in a good agreement with the modern warming phase (**U**, Fig. 7) started soon after the end of the Little Ice Age (ca. 1860). **T5** cycle seems to be mainly controlled by climatic factors (allocyclic nature) and the flooding surface may represent a true shoreline inland migration. The reconstructed post LIA sea level rise of about 0.5 m seems to be demonstrated by subaerial use of the wood palisade before modern times.

6. Conclusions

The Mistras coastal barrier evolution was controlled by four sea level fluctuations. It started to develop as regressive system (**T1**) about 6355±67 cal y BP when the post Late Glacial Maximum sea level rise decelerated. At that time, Holocene Climate Optimum, sea level was at about 2 m below the present. Between 6000 and 3000 cal y BP sea level fell of at least 5 m allowing the erosion of most of the previous formed barrier system and the migration of the coast seaward of about 1 km. In this time interval, the Mistras area was influenced by river systems feeding the pre-existing lagoon.

Around 3000 cal y BP sea level rose again reaching at about 2450±90 cal y BP the present high (cycle **T2**). This sea level highstand occurred during the Warm Roman time and represents the time during which the modern coastal barrier systems started to form. A new coastal barrier developed as a spit system growing toward the ENE and delimiting on its northern side a sheltered lagoon. Phoenician were living at that time in the Tharros/Mistras area. Up to now, there is no archaeological evidence that these Phoenician traders built a harbour or docs, and boats were most probably anchored in front of the beach. It is worthy to note that archaeological findings become younger in the same direction of the spit progradation.

From 525 BC (2540 years BP) Tharros become an important Punic colony. Boats carrying goods needed to be protected and, from at least the 4th Century BC (2400-2300 years BP), an artificial barrier was built connecting the small sandy islands of the sheltered lagoon. The barrier, however, also acted as preferential accumulation place of the sand carried by the small rivers. During the Imperial Roman time (since 2000 years BP) the lagoon silted and Roman had to move the harbour more seaward, probably in front of the city of Tharros.

Around 1998±99 cal y BP sea level fell again up to a minimum of 4 m. The well-preserved and continuous lag found at the base of cycle **T3** indicates that sea level oscillation was big enough to rework part of the previous formed beach, including pottery fragments and bones. This climatic change was the last able to consistently influence the Mistras coastal barrier system evolution.

Approximately since 1341±43 cal y BP, during the Medieval Warm Time, the Mistras system evolved as barrier lagoon (**T3-T4**). The presence of the structures built by the Punics allowed sediments being trapped in front of them and changing the system from spit to barrier lagoon. The continuous sea level fall (up to 0.5 m) occurred during the Little Ice Age allowed the system prograding quasi continuously for about 1200 years.

The new sea level rise occurred after 1850 AD brought the sea at the present high and allowed the development of the uppermost **T5** cycle.

Four on five recognized flooding surfaces can be tied with eustatic and/or climatic peaks supporting the evidence that low sediment supply coastal areas are good sites where tentatively link small-scale T-R cycles with allocyclic factors.

At least 3 very high frequency T-R cycles (T2, T3, T5) seems to represent "true" small amplitude (less than 10 meters) drops and rises of the sea level and can be used to better model the Middle-Late Holocene eustatic fluctuations at regional and possibly at supraregional scale. Moreover, also considering the ^{14}C errors, it seems that the all recognized coastal regressions occurred during receding phases of warm times.

Concluding remarks are that geological and archaeological data indicate that the Mistras barrier lagoon evolution was human influenced since the Punic period. The study pointed that little human activities on the coast could influence its natural behaviour and landscape, and that little climatic changes both positive and negative can induce progradation or erosion of the system as well.

Acknowledgment

The authors are indebted with Alessandro Amorosi and an anonymous reviewer that strongly improved with their comments the final version of the manuscript. We kindly acknowledge Francesco Cubeddu for the aerial pictures of the underwater wall (Fig. 4), the team of the University of Cagliari and of the Archaeological Superintendence of Cagliari and Oristano that worked on the archaeological excavations, Matteo Rosa and Paola Zoccheddu that helped with the GPR survey and field analysis. The work has been founded with grant Legge Regionale 7/2007 Project: "Variazioni climatiche, modificazioni del paesaggio ed impatto antropico in aree costiere ed interne della Sardegna tra preistoria e storia", founded by Regione Autonoma della Sardegna, (RAS, Assessorato della Programmazione, Bilancio, Credito e Assetto del Territorio (Base Research Project, L.R. 7 agosto 2007, n. 7, Bando 2008, anni 2010-2012, Resp. Carla Del Vais). Partial found to VP has been provided by the Russian Government Program of Competitive Growth of Kazan Federal University.

REFERENCES

Acquaro, E., Mezzolani, A., 1995. Tharros. Itinerari, XVII. Istituto Poligrafico e Zecca dello Stato, Roma, 108 pp.

Acquaro, E., Marcolongo, B., Vangelista, F., Verga, F. Eds, 1999. Il *Portto buono* di Tharros. Studi e ricerche sui Beni Culturali, 2. La Spezia, 33 pp.

Amorosi, A., Centineo, M.C., Colalongo, M.L., Fiorini, F., 2005. Millennial-scale depositional cycles from the Holocene of the Po plain, Italy. Marine Geology, 222-223, 7-18.

Amorosi, A., Ricci Lucchi, M., Rossi, V., Sarti, G., 2009. Climate change signature of small-scale parasequences from LateglacialeHolocene transgressive deposits of the Arno valley fill. Palaeogeography, Palaeoclimatology, Palaeoecology, 273, 142-152.

Amorosi, A., Bruno, L., Campo, B., Morelli, A., Rossi, V., Scarponi, D., Hong, W., Bohacs, K.M., Drexlercet, T.M., 2017. Global sea-level control on local parasequence architecture from the Holocene record of the Po Plain, Italy. Marine and Petroleum Geology, 87, 99-111.

Andreucci, S., Pascucci, V., Murray, A.S., Clemmensen, L.B., 2009. Late Pleistocene coastal evolution of San Giovanni di Sinis (west Sardinia, Western Mediterranean). Sedimentary Geology, 216, 104-116.

Andreucci, S., Sechi, D., Buylaert, J.P, Sanna, L., Pascucci, V., in press. Post-IR IRSL290 dating of K-rich feldspar sand grains in a wind-dominated system on Sardinia. Marine and Petroleum Geology, 87, 91-98.

Antonioli, F., Lo Presti, V., Rovere, A., Ferranti, L., Anzidei, M., Furlani, S., Mastronuzzi, G., Orrù, P.E., Scicchitano, G., Sannino, G., Spampinato, C.R., Pagliarulo, R., Deiana, G., de Sabatam, E., Sansòn, P., Vacchi, M., Vecchio, A., 2015. Tidal notches in Mediterranean Sea: a comprehensive analysis. Quaternary Science Reviews, 119, 66-84.

Antonioli, F., Anzidei, M., Amorosi, A., Lo Presti, V., Mastronuzzi, G., Deiana, G., De Falco, G., Fontana, A., Fontolan, G., Lisco, S., Marsico, A., Moretti, M., Orrù, P.E., Sannino, G.M., Serpelloni, E., Vecchio, A., 2017. Sea-level rise and potential drowning of the Italian coastal plains: Flooding risk scenarios for 2100. Quaternary Science Reviews, 158, 29-43.

Atzeni, A., Pani, D., Ibba, N., 2007. Sinis Peninsula (Western Sardinia, Italy) coastal system analysis through hydrodynamic and remote-sensing techniques. Special Paper of the Geological Society of America, 426, 189-197.

Baroni, C., Orombelli, G., 1996. The Alpine Iceman and Holocene Climatic Change. Quaternary Research, 46, 78-83.

Bernal Casasola, D., 2010. Arqueología de los puertos romanos del Fretum Gaditanum: nuevos datos, nuevas perspectivas. Bollettino di Archeologia on line, http://www.bollettinodiarcheologiaonline.beniculturali.it/documenti/generale/7_BernalCasasola_paper.pdf.

Bond, G., Showers, W., Cheseby, M., Lotti, R., Almasi, P., deMenocal, P., Priore, P., Cullen, H., Hajdas, I., Bonani, G., 1997. A pervasive millennial-scale cycle in North Atlantic Holocene and glacial climates. Science, 278, 1257-1266.

Boyer, J., Duvail, C., Le Strat, P., Gensous, B., Tesson, M., 2005. High resolution stratigraphy and evolution of the Rhône delta plain during postglacial time, from subsurface drilling data bank. Marine Geology, 222-223, 267-298.

Büntgen, U., Tegel, W., Nicolussi, K., McCormick, M., Frank, D., Trouet, V., Kaplan, J.O., Herzig, F., Heussner, K.U., Wanner, H., Luterbacher, J., Esper, J., 2011. 2500 Years of European Climate Variability and Human Susceptibility. Science, 331, 578-582.

Carboni, S., Lecca, L., 1995. The Pliocene of Capo Mannu (western Sardinia): marine littoral-continental dune transition. Comptes Rendus. Académie des Sciences, Serie II: Sciences de la Terre et des Planetes, 320, 1203-1210.

Carboni, S., Lecca, L., Hillaire-Marcel, C., Ghaleb, B., 2014. MIS 5e at San Giovanni di Sinis (Sardinia, Italy): Stratigraphy, U/Th dating and “eustatic” inferences. Quaternary International, 328-329, 21-30.

Carmignani, L., Barca, S., Oggiano, G., Pertusati, P.C., Salvadori, I., Conti, P., Eltrudis, A., Funedda, A., Pasci, S., 2001. Note illustrative della Carta Geologica della Sardegna a scala 1:200.000. Memorie descrittive Carta Geologica Italiana, 60. Istituto Poligrafico e Zecca dello Stato, Roma, 283 pp.

Casula, G., Cherchi, A., Montadert, L., Murru, M., Sarria, E., 2001. The Cenozoic grabens system of Sardinia: geodynamic evolution from new seismic and field data. Marine and Petroleum Geology, 18, 863-888.

Cherchi, A., Montadert, L., 1982. Oligo-Miocene rift of Sardinia and the early history of the Western Mediterranean Basin. Nature, 298 (5876), 736-739.

Christiansen, B., Ljungqvist, F.C., 2012. The extra-tropical Northern Hemisphere temperature in the last two millennia: reconstructions of low-frequency variability. Climate of the Past, 8, 765-786.

Clemmensen, L.B., Richardt, N., Andersen, C., 2001. Holocene sea-level variation and spit development: data from Skagen Odde, Denmark. The Holocene, 11, 323-331.

Davis, R.A., Clifton, H.E., 1987. Sea-level change and the preservation potential of wave-dominated and tide-dominated coastal sequences. In: Sea-Level fluctuation and Coastal Evolution (D. Nummedale, O.H. Pilkey, and J.D. Howard Eds.), SEPM Special Publications, 11, 166-178, Tulsa, OK.

Davis, R.A., Duncan, M.F., 2004. Beaches and coasts, Balckwell Science Ltd., Oxford, UK, 419 pp.

Davis, B.A.S., Brewer, S., Stevenson, A.C., Guiot, J., 2003. The temperature of Europe during the Holocene reconstructed from pollen data. Quaternary Science Reviews, 22, 1701-1716.

Dean, W.E., 1974. Determination of Carbonate and Organic Matter in Calcareous Sediments and Sedimentary Rocks by Loss on Ignition: Comparison with other methods. Journal of Sedimentary Petrology, 44, 242-248

De Falco, G., Molinaroli, E., Baroli, M., Bellacicco, S., 2003. Grain size and compositional trends of sediments from Posidonia oceanica meadows to beach shore, Sardinia, western Mediterranean. Estuarine, Coastal and Shelf Science, 58, 299-309.

De Falco, G., Baroli, M., Cucco, A., Simeone, S., 2008. Intrabasinal condition promoting the development of a biogenic carbonate sedimentary facies associated with the seagrass Posidonia oceanica. Continental Shelf Research, 28, 797-812.

De Falco, G., Antonioli, F., Fontolan, G., Lo Presti, V., Simeone, S., Tonielli, R., 2015. Early cementation and accommodation space dictate the evolution of an overstepping barrier system during the Holocene. Marine Geology, 369, 52-66.

Del Vais, C., 2014. Il Sinis di Cabras in età punica. In: Le sculture di Mont’e Prama. Contesto, scavi e materiali (M. Minoja and A. Usai Eds). Roma, pp. 103-136.

Del Vais, C., 2015. Laguna di Mistras. FastiOnline Excavations, http://www.fastionline.org/excavation/micro_view.php?item_key=fst_cd&fst_cd=AIAC_3120.

Del Vais, C., Depalmas, A., Fariselli, A.C., Melis, R.T., Pisanu, G., 2008. Ricerche geo-archeologiche nella Penisola del Sinis (OR): aspetti e modificazioni del paesaggio tra preistoria e storia. In: Atti del II Simposio Il monitoraggio costiero mediterraneo: problematiche e tecniche di misura (Napoli, 4-6 giugno 2008). CNR-IBIMET, Firenze, pp. 403-414.

Del Vais, C., Fariselli, A.C., Melis, R.T., Pisanu, G., Sanna, I., 2010. Ricerche e scavi subacquei nella laguna di Mistras (Cabras-OR). ArcheoArte, 1, 299-300, http://ojs.unica.it/index.php/archeoarte/article/view/54/37.

Depalmas, A., Melis, R.T., 2010. The Nuragic People: Their Settlements, Economic Activities and Use of the Land, Sardinia, Italy. In: Landscapes and Societies (I.P. Martini and W. Chesworth Eds), Springer Science+Business Media B.V., Dordrecht Heidelberg London New York, pp. 177-186.

Di Rita, F, Simone, O., Caldara, M., Gehrels, W.R., Magri, D., 2011. Holocene environmental changes in the coastal Tavoliere Plain (Apulia, southern Italy): a multiproxy approach. Palaeogeography, Palaeoclimatology, Palaeoecology, 310, 139-151.

Di Rita, F., Melis, R.T., 2013. The cultural landscape near the ancient city of Tharros (central West Sardinia): Vegetation changes and human impact. Journal of Archaeological Science, 40, 4271-4282.

Duncan, R., Ginesu, S., Secchi, F., Sias, S., 2011. The recent evolution of the Sinis region (Western coast of Sardinia, Italy) on the basis of new radiometric data of the Pliocenic volcanism. Geografia Fisica e Dinamica Quaternaria, 34, 175-181.

Esper, J., Cook, E.R., Schweingruber, F.H., 2002. Low-frequency signals in long tree-ring chronologies for reconstructing past temperature variability. Science, 295, 2250-2253.

Fagan, B.M., 2000. The Little Ice Age: how climate made history, 1300-1850. Basic Books, New York, 272 pp.

Fleming, K., Johnston, P., Zwartz, D., Yokoyama, Y., Lambeck, K., Chappell, J., 1998. Refining the eustatic sea-level curve since the Last Glacial Maximum using far- and intermediate-field sites. Earth and Planetary Science Letters, 163, 327-342.

Forti, S., Orrù, P.E., 1995. Geomorfologia costiera e marina della Penisola del Sinis (Sardegna Occidentale). Bollettino della Società Geologica Italiana, 114, 3-21.

Fruergaard, M., Møller, I., Johannessen, P.N., Nielsen, L.H., Andersen, T.J., Nielsen, L.H., Sander, L., Pejrup, M., 2015a. Stratigraphy, Evolution, And Controls Of A Holocene Transgressive-Regressive Barrier Island Under Changing Sea Level: Danish North Sea Coast. Journal of Sedimentary Research, 2015, 820-844.

Fruergaard, M., Andersen, T.J., Nielsen, L.H., Johannessen, P.N., Aagaard, T., Pejrup, M., 2015b. High-resolution reconstruction of a coastal barrier system: impact of Holocene sea-level change. Sedimentology, 62, 928-969.

Galili, E., Zviely, D., Weinstein-Evron, M., 2005. Holocene sea-level changes and landscape evolution on the northern Carmel coast (Israel). Méditerranée, 1.2.

Galili, E., Rosen, B., Stern, E.J., Finkielsztejn, G., Kool, R., Bahat-Zilberstein, N., Sharvit, Y., Kahanov, Y., Friedman, Z., Zviely, D., 2007. New insights on Maritime Akko revealed by underwater and coastal archaeological research. In: Israeli Society for Aquatic Sciences. Forth annual meeting (30-5-2007), Haifa University, pp. 64-74.

Galili, E., Rosen, B., Zviely, D., Silberstein, N., Finkielsztejn, G., 2010. The Evolution of Akko Harbor and its Mediterranean Maritime Trade Links. Journal of Island & Coastal Archaeology, 5, 2, 191-211.

Goy, J.L., Zazo, C., Dabrio, C.J., 2003. A beach-ridge progradation complex reflecting periodical sea-level and climate variability during the Holocene (Gulf of Almería, Western Mediterranean). Geomorphology, 50, 251-268.

Gueguen, E., Doglioni, C., Fernández, M., 1998. On the post-25 Ma geodynamic evolution of the western Mediterranean. Tectonophysics, 298, 259-269.

Grant, K.M., Rohling, E.J., Bar-Matthews, M., Ayalon, A., Medina-Elizalde, M., Bronk Ramsey, C., Satow, C., Roberts, A.P., 2012. Rapid coupling between ice volume and polar temperature over the past 150 kyr. Nature, 491, 744-747.

Lambeck, K., Antonioli, F., Purcell, A., Silenzi, S., 2004. Sea-level change along the Italian coast for the past 10,000 yr. Quaternary Science Reviews, 23, 1567-1598.

Lambeck, K., Antonioli, F., Anzidei, M., Ferranti, L., Leoni, G., Scicchitano, G., Silenzi, S., 2011. Sea level change along the Italian coast during the Holocene and projections for the future. Quaternary International, 232, 250-257.

Lecca, L., Scarteddu, R., Secchi, F., 1983. La piattaforma continentale Sarda da Capo Mannu a Capo Marrargiu. Bollettino della Società Geologica Italiana, 102, 57-86.

Mimura, N., 2013. Sea-level rise caused by climate change and its implications for society. Proc Jpn Acad Ser B Phys Biol Sci., 89, 281–301.

Le Roy Ladurie, E., 1959. Historie et Climat. Annales Economies, Sociétés, Civilisations, 14, 1, 3-34.

Longhitano, S.G., Della Luna, R., Milone, A.L., Cilumbriello, A., Caffau, M., Spilotro, G., 2016. The 20,000-years-long sedimentary record of the Lesina coastal system (southern Italy): From alluvial, to tidal, to wave process regime change. Holocene, 26, 678-698.

Lowrie, A., Hamiter, R., 1995. Fifth and sixth order eustatic events during Holocene (fourth order) highstand influencing Mississippi delta-lobe switching. Journal of Coastal Research, Special Issue 17, 225-229.

Martin, R.E., Leorri, E., McLaughlin, P.P., 2007. Holocene sea level and climate change in the Black Sea: Multiple marine incursions related to freshwater discharge events. Quaternary International, 167-168, 61-72.

McCormick, M., Büntgen, U., Cane, M.A., Cook, E.R., Harper, K., Huybers, P.J., Litt, T., Manning, S.W., Mayewski, P.A., More, A.F.M., Nicolussi, K., Tegel., W., 2012. Climate Change during and after the Roman Empire: Reconstructing the Past from Scientific and Historical Evidence. Journal of Interdisciplinary History, 43, 169-220.

Magny, M., Combourieu Nebout, N., 2013. Holocene changes in environment in the Mediterranean. Climate of the Past, 9, 1447-1454.

Melis, R.T., Depalmas, A., Di Rita, F., Montisa, F., Vacchi, M., 2017. Mid to late Holocene environmental changes along the coast of western Sardinia (Mediterranean Sea). Global and Planetary Change, 155, 29-41.

Mensing, S.A., Tunno, I., Sagnotti, L., Florindo, F., Noble, P., Archer, C., Zimmerman, S., Pavon-Carrasco, F.J., Cifani, G., Passigli, S., Piovesan, G., 2015. 2700 years of Mediterranean environmental change in central Italy: a synthesis of sedimentary and cultural records to interpret past impacts of climate on society. Quaternary Science Reviews, 116, 72-94.

Milli, S., Mancini, M., Moscatelli, M., Stigliano, F., Marini, M., Cavinato, G.P., 2016. From river to shelf, anatomy of a high-frequency depositional sequence: the Late Pleistocene to Holocene Tiber depositional sequence. Sedimentology, 63, 1886-1928.

Morhange, C., Laborel, J., Hesnard, A., 2001. Changes of relative sea level during the past 5000 years in the ancient harbor of Marseille, Southern France. Palaeogeography, Palaeoclimatology, Palaeoecology, 166, 319-329.

Morhange, C., Marriner, N., Carayon, N., 2014. The geoarchaeology of ancient Mediterranean harbours. In: La géoarchéologie française au XXI[e] siècle (N. Carcaud and G. Arnaud-Fassetta Eds). CNRS, Paris, pp. 245-254.

Nielsen, L., Clemmensen, L.B., 2009. Sea-level markers identified in ground-penetrating radar data collected across a modern beach ridge system in a microtidal regime. Terra Nova, 21, 474-479.

Pascucci, V., Martini, I.P., Endres A., 2009. Facies and Ground-penetrating-radar (GPR) characteristics of coarse-grained beach deposits of the uppermost Pleistocene glacial Lake Algonquin, Ontario Canada. Sedimentology, 56, 529-545.

Pascucci, V., Sechi, D., Andreucci, S., 2014. Middle Pleistocene to Holocene coastal evolution of NW Sardinia (Mediterranean Sea, Italy). Quaternary International, 328-329, 3-20.

Patacca, E., Sartori, R., Scandone, P., 1990. Thyrrhenian basin and Apenninic arcs: Kinematic relations since late Tortonian times. Memorie della Società Geologica Italiana, 45, 425-451.

Perry, C.A., Hsu, K.J., 2000. Geophysical, archaeological, and historical evidence support a solar-output model for climate change. Proceedings of the National Academy of Science, 97, 12433-12438.

Pittau, P., Ługliè, C., Buosi, C., Sanna, I., Del Rio, M., 2012. Palynological interpretation of the Early Neolithic coastal open-air site at Sa Punta (central-western Sardinia, Italy). Journal of Archaeological Science, 39, 1260-1270.

Reimer, P.J., Bard, E., Bayliss, A., Beck, J.W., Blackwell, P.G., Bronk Ramsey, C., Buck, C.E., Cheng, H., Edwards, R.L., Friedrich, M., Grootes, P.M., Guilderson, T.P., Haflidason, H., Hajdas, I., Hatté, C., Heaton, T.J., Hoffmann, D.L., Hogg, A.G., Hughen, K.A., Kaiser, K.F., Kromer, B., Manning, S.T., Niu, M., Reimer, R.W., Richards, D.A., Scott, E.M., Southon, J.R., Staff, R.A., Turney, C.S.M., van der

Plicht, J., 2013. IntCal13 and Marine13 Radiocarbon Age Calibration Curves 0–50,000 Years cal BP. Radiocarbon, 55, 1869-1887.

Reinson, G.E., 1992. Transgressive barrier island and estuarine systems. In: Facies Models – Response to sea Level Change (R.G. Walker and N.P. James Eds). Geological Association of Canada, St. John's, NFL, pp. 179-194.

Ribotti, A., De Falco, G., Arrichiello, V., 2002. Experimentation of an innovative Lagrangian coastal drifter. Elsevier Oceanography Series, 66 (C), 335-340.

Roberts, N., Meadows, M.E., Dodson, J.R., 2001. The history of Mediterranean-type environments: climate, culture and landscape. Holocene, 11, 631-634.

Roberts, N., Brayshaw, D., Kuzucuoglu, C., Perez, R., Sadori, L., 2011. The mid-Holocene climatic transition in the Mediterranean: causes and consequences. Holocene, 21, 3-14.

Rohling, E.J., De Rijk, L.S., 1999. Holocene Climate Optimum and Last Glacial Maximum in the Mediterranean: the marine oxygen isotope record. Marine Geology, 153, 57-75.

Rydin, H., Jeglum, J.K., 2013. The Biology of Peatlands, 2Eds. Oxford University Press. Oxford UK, 432 pp.

Salvi, D., 1991. Contributo per la ricostruzione topografica della Cagliari punica. Notizie preliminari sullo scavo di S. Gilla 1986-1987. In: Atti del II Congresso Internazionale di Studi Fenici e Punici (Roma, 9-14 novembre 1987). CNR, Roma, pp. 1215-1220.

Salvi, D., 2014. Cagliari: Santa Gilla, la laguna e l'argilla. ArcheoArte, 3, 213-235, http://ojs.unica.it/index.php/archeoarte/article/view/955.

Simeone, S., De Falco, G., 2012. Morphology and composition of beach-cast *Posidonia oceanica* litter on beaches with different exposures. Geomorphology, 151-152, 224-233.

Sivan, D., Wdowinski, S., Lambeck, K., Galili, E., Raban, A., 2001. Holocene sea-level changes along the Mediterranean coast of Israel, based on archaeological observations and numerical model. Palaeogeography, Palaeoclimatology, Palaeoecology, 167, 101-117.

Somoza, L., Barnolas, A., Arasa, A., Maestro, A., Rees, J.G., Hernández-Molina, F.J., 1998. Architectural stacking patterns of the Ebro delta controlled by Holocene high-frequency eustatic fluctuations, delta-lobe switching and subsidence processes. Sedimentary Geology, 117, 11-32.

Soro, L., Sanna, I., in press. Merci e approdi nella marina di Cagliari: il quadro archeologico subacqueo. In: Archeologia urbana a Cagliari. Scavi nella chiesa di Sant'Eulalia alla Marina 1. il quartiere dalle origini ai giorni nostri: *status quaestionis* all'inizio della ricerca (R. Martorelli and D. Mureddu Eds).

Spanu, P.G., 1998. La Sardegna bizantina tra VI e VII secolo. Mediterraneo Tardoantico e Medievale. Scavi e Ricerche, 12. Oristano, 263 pp.

Spanu, P.G., and Zucca, R., 2011. Da Τάρραι πόλις al *portus sancti Marci*: storia e archeologia di una città portuale dall'antichità al Medioevo. In: *Tharros Felix* 4 (A. Mastino, P.G. Spanu, A. Usai, R. Zucca Eds). Roma, pp. 15-103.

Stranne, C., Jakobsson, M., Björk, G., 2014. Arctic Ocean perennial sea ice breakdown during the Early Holocene Insolation Maximum. Quaternary Science Reviews, 92, 123-132.

Stuiver, M., Reimer, P.J., Reimer, R.W., 2017. CALIB 7.1 [WWW program] at http://calib.org.

Tigny, V., Ozer, A., De Falco, G., Baroli, M., Djenidi, S., 2007. Relationship between evolution of the shoreline and the *Posidonia oceanica* meadow limit in a Sardinian Coastal Zone. Journal of Coastal Research, 23, 787-793.

Tanabe, S., Nakanishi, T., Ishihara, Y., Nakashima, R., 2015. Millennial-scale stratigraphy of a tide-dominated incised valley during the last 14 kyr: spatial and quantitative reconstruction in the Tokyo Lowland, central Japan. Sedimentology, 62, 1837-1872.

Törnqvist, T.E., Hijma, M.P., 2012. Links between early Holocene ice-sheet decay, sea-level rise and abrupt climate change. Nature Geoscience, 5, 601-606.

Usai, A., 2014. Alle origini del fenomeno di Mont'e Prama. La civiltà nuragica nel Sinis. In: Le sculture di Mont'e Prama. Contesto, scavi e materiali (M. Minoja and A. Usai Eds). Roma, pp. 29-72.

Vacchi, M., Marriner, N., Morhange, C., Spada, G., Fontana, A., Rovere, A., 2016. Multiproxy assessment of Holocene relative sea-level changes in the western Mediterranean: Sea-level variability and improvements in the definition of the isostatic signal. Earth-Science Reviews, 155, 172-197.

Van de Noor, R., 2013. Climate Change Archaeology: Building Resilience from Research in the World's Coastal Wetlands. Oxford University Press, Oxford, UK, 272 pp.

Vink, A., Steffen, H., Reinhardt, L., Kaufmann, G., 2007. Holocene relative sealevel change, isostatic subsidence and the radial viscosity structure of the mantle of northwest Europe (Belgium, the Netherlands, Germany, southern North Sea). Quaternary Science Reviews, 26, 3249-3275.

Walsh, K., 2014. The Archaeology of Mediterranean Landscapes: Human-Environment Interaction. Cambridge University Press, 365 pp.

Wanner, H., Beer, J., Bütikofer, J., Crowley, T.J., Cubasch, U., Flückiger, J., Goosse, H., Grosjean, M., Joos, F., Kaplan, J.O., Küttel, M., Müller, S., Prentice, I.C., Solomina, O., Stocker, T.F., Tarasov, P., Wagner, M., Widmann, M., 2008. Mid- to late Holocene climate change: an overview. Quaternary Science Reviews, 27, 1791-1828.

Weidman, C.R., Ebert, J.R., 1993. Cyclic spit morphology in a developing inletsystem. In: Formation and Evolution of Multiple Tidal Inlet Systems (D.G. Aubrey and G.S. Giese Eds). American Geophysical Union, Washington D.C., 44, 158-185.

Zanchetta, G., Van Welden, A., Baneschi, I., Drysdale, R., Sadori, L., Roberts, N., Giardini, M., Beck, C., Pascucci, V., Supplizio, R., 2012. Multiproxy record for the last 4500 years from Lake Shkodra (Albania/Montenegro). Journal of Quaternary Science, 27, 780-789.

Zazo, C., Dabrio, C.J., Goy, J.L., Lario, J., Cabero, A., Silva, P.G., Bardajı´, T., Mercier, N., Borja, F., Roquero, E., 2008. The coastal archives of the last 15 ka in the Atlantic–Mediterranean Spanish linkage area: Sea level and climate changes. Quaternary International, 181, 72–87

CAPTION TO FIGURES

Table 1

AMS ^{14}C radiocarbon age dating. The radiocarbon ages were calibrated using CALIB 7.04 (Stuiver et al., 2017), and Marine13 (Reimer et al., 2013) Calibration Curves 0–50,000 cal y BP. Samples S1-10 are from the wells; Samples C1, C2, C3 come from the underwater archaeological excavation (UWE1); US21-SE, US26-SE, US35-SE from archaeological excavation (site C).

Table 2

Grain size analysis (percentage) of sediments collected along the core profiles used for statistical analysis. Mean and standard deviation (sd) are the used values.

Fig. 1 The studied area. A) Satellite view of the Mediterranean region where Sardinia occupies a central position. Dashed line indicates the Sardinia anticlockwise rotation occurred in the Neogene time; B) Digital terrain model of south Sardinia; in the map are reported the main cities of the central southern part of the island, the Campidano graben and in the red square close to Oristano (west side) the Sinis Peninsula where Mistras-Tharros area is located; C) Satellite view (from Google earth) of the Sinis Peninsula. In the right upper part is the Mistras lagoon and the studied coastal barrier system, the Sinis Peninsula and in the red circle Tharros; D) Tharros Punic-Roman ruins.

Fig. 2 Digital Terrain Model (elevation is 1 m step) of the Mistras coastal barrier system. In the map are reported the location of the 11 drilled wells, archaeological excavations (A, B, C) and ages of the remains found (7^{th}-3^{rd} centuries) in the sites B and C respectively, Ground Penetrating Radar profiles, the Punic walls, and the trace of figure 7 cross section. Note, that all wells are plotted on the cross section following the beach ridges morphology. GPR17 is the radar profile presented in Fig. 8. MTR1 indicates the location of the well published by Di Rita and Melis, 2012.

Fig. 3 Sedimentary facies of the 82 sediment samples taken in the 11 wells (see supplementary material) ordered according to 9 variables: gravel%, coarse sand%, Total Organic Carbon (TOC)%, $CaCO_3$ content, medium-fine sand%, mean diameter (phi), silt%, clay% and sorting.

Factor 1 (40% of the variance) was positively correlated to Fine fraction (Silt%, Clay%), organic matter % and sorting coefficient, and muddy organic sediments were separated from sandy sediments. These have been interpreted as shoreface/inner bay deposits.

Factor 2 (35% of the variance) is positively correlated to Gravel % and Coarse Sand % and inversely correlated to Medium-Fine sands, Mean Diameter and $CaCO_3$ content. Factor 2 separates gravelly and coarse sandy sediments from medium-fine sands interpreted respectively as Foreshore/Transgressive Lag and as Backshore deposits.

Fig. 4 The sandstone blocks wall and the basalt boulder structure. The sandstone wall was made probably during 4^{th}-3^{rd} Century BC and reinforced with wood palisade probably during 2nd-1st Century BC (AMS ^{14}C radiocarbon age dating ranges between 2184±127 and 1998±99 cal y BP). A) Location of the structures (satellite image from Google Earth); B) Detailed image of the sandstone wall and location of section A-A' (aerial photo is courtesy of F. Cubeddu); C) A-A', Cross-section transversal to the sandstone wall. The section has been realized after the underwater excavation (A of Fig. 2) conducted in 2009 on the wall. UWE1 and UWE2 are vertical underwater excavation of about 1.2 m made on both sides of the wall; D) The basalt boulder structure under the lagoon surface. It was possibly built in Punic time to protect the boats anchored in the inner lagoon.

Fig. 5 The coastal barrier deposits excavated during the archaeological digs. A) The excavation of the 2014 (B of Fig. 2) (dig is 2.3 m deep), solid-point white line indicates the boundary between shoreface (*SF*) and foreshore (*FS*) deposits. An arrow indicates the alternation of silt to fine sand and organic rich layers (made of *Posidonia oceanica*) fragments. In the upper part of the picture, covered by white bags, is reported the insert presented in C; B) the excavation of 2015 (C of Fig. 2), dig is 1.07 m deep; shoreface (*SF*) and foreshore (*FS*) deposits encountered during excavation.

Note the strata encountered in both excavations, from 0 to 1 m (B - on 2014) and from 0 to 0.5 m (C - in 2015) below the surface, the foreshore deposits dipping 5° toward the E (open sea); C) Detail of the foreshore sediments. The withe lines enhance the foreshore strata dip; D) Foreshore is composed of medium to coarse, well-sorted sand with sparse pebbles (volcanic and pottery) and shell fragments (scale is 30 cm).

Fig. 6 Cross-section of the Mistras coastal barrier system. The section has been realized projecting most of the wells drilled in the area (see Fig. 2). T1-T5 are the T-R cycles, in read the bounding surfaces (transgressive surfaces). Yellow solid dots: archaeological data from pottery findings referred to Phoenician and Punic time (7^{th}-3^{rd} Century) (sherds of transport amphorae and plain ware pottery); Black solid dots: AMS ^{14}C Radiocarbon dating in Median calendar ages (year BP) 2σ errors (cal y BP), complete values are in table 1. Abbreviations: m=mud, s=sand, g=gravel, apsl=above present sea level, psl=present sea level. Note that deposits of the foreshore and backshore have been grouped under the label beachface.

Fig. 7 Proposed Holocene sea level curve (solid red, the red dashed part represents uncertainties). The curve is plotted together with the global solar output (SA, in green) and sea level curves (SC, dashed black) proposed by Perry and Hsu (2000) based on geophysical, archaeological, and historical evidences, Grant et al. (2012) for the Red Sea (dashed blue), and Lambeck et al. (2004) for the Mediterranean Sea (solid black). Note how the proposed sea level curve is interested by high frequency fluctuations from 2500 y BP up to Present. The yellow square refers to archaeological ages; the green square refers to ^{14}C ages in cal y BP. In both cases, the dimension of the square is representative of the 2σ error considered as maximum and minimum ages.

Fig. 8 Uniterpreted (above) and interpreted (line drawing) 200 MHz Ground Penetrating Radar profile GPR17 (location is in Fig. 2). **sfs**= sharp flooding surfaces; that is, transgressive-regressive cycles bounding surface; **mfs**= maximum flooding surfaces defining the switch from transgression to regression of the barrier coastal systems. Note the shallowing-upward trend of both T1 and T2 cycles.

Fig. 9 Reconstruction of the evolution of the Mistras coastal barrier system since beach regression of **T2** cycle; that is, since about 2500 cal y BP when sea level rise reached the present high. A) Evolution of the costal barrier system on a satellite image photomosaic (from Google earth): solid red lies indicate the T-R cycles boundaries, dashed red lines indicate how the system prograded (regressive phase). Note that from **T3** (about 1300 cal y BP) the system evolution switched from spit to barrier lagoon. This new evolution was controlled by the Punic walls (black dashed line) built during around 2400-2300 cal y BP (and maintained until 2000 years BP) to protect the lagoon L2 used as harbour. In brackets, for each well, is provided the elevation in meter above the present sea level; B) Cartoon (not to scale) imaging the 2D evolution of the Mistras system along and ideal WNW-ESE cross section from 2500 cal y BP to the Present.

Supplementary materials

Supplementary S1. Detail description and facies analysis of the wells S2, S1 (location in Fig. 2). For each log are reported the coordinates, a short description of the facies, the location and depth (black dots) of samples used for ^{14}C ages (i.e. S2_224, means that the sample has been taken at depth from the surface of 2.24 meters) and the sediment grain size histograms. Note that:

S2(1)C1-16 are samples numbers. Note that the first 20 cm of sediments encountered in the well S2 and referred to lagoon have not been discussed in the text. These, also on the base of the archaeological excavation, are referred to the modern lagoon deposits of Mistras.

Supplementary S2. Detail description and facies analysis of the wells S6, S3 (location in Fig. 2). For each log are reported the coordinates, a short description of the facies, the location and depth (black dots) of samples used for ^{14}C ages (i.e. S6_339, means that the sample has been taken at depth from the surface of 3.39 meters) and the sediment grain size histograms. Note that: S6(3)C1-12 are samples numbers.

Supplementary S3. Detail description and facies analysis of the wells S4, S5 (location in Fig. 2). For each log are reported the coordinates, a short description of the facies, the location and depth (black dots) of samples used for ^{14}C ages (i.e. S4_340, means that the sample has been taken at depth from the surface of 3.40 meters) and the sediment grain size histograms. Note that: S4(5)C1-11 are samples numbers.

Supplementary S4. Detail description and facies analysis of the wells S7, S10 (location in Fig. 2). For each log are reported the coordinates, a short description of the facies, the location and depth (black dots) of samples used for ^{14}C ages (i.e. S7_349, means that the sample has been taken at depth from the surface of 3.49 meters) and the sediment grain size histograms. Note that: S7(10)C1-14 are samples numbers.

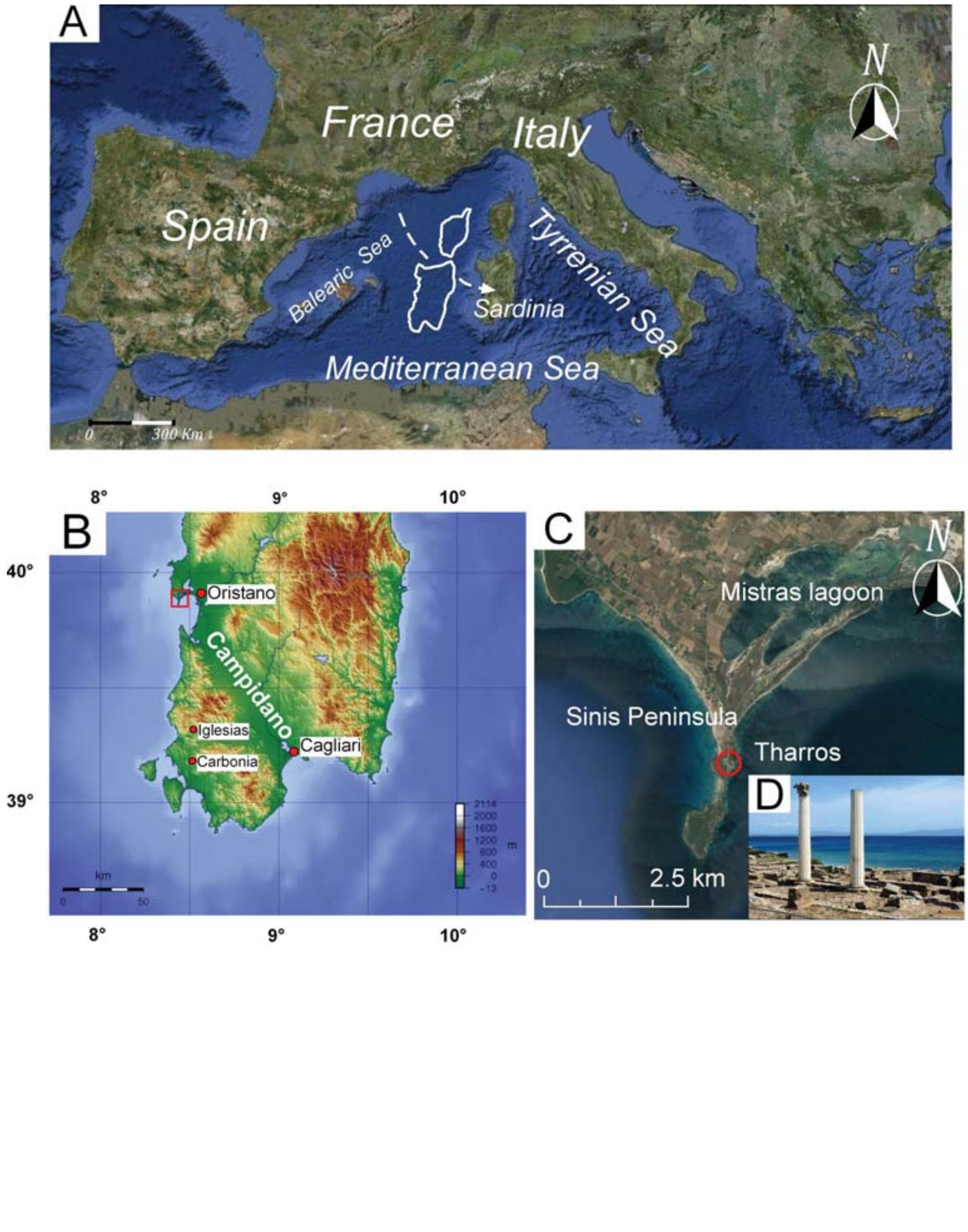
A
N
France
Italy
Spain
Balearic Sea
Sardinia
Tyrrenian Sea
Mediterranean Sea
0
300 Km
B
8°
9°
10°
40°
39°
Oristano
Campidano
Iglesias
Carbonia
Cagliari
km
0
50
2114
2000
1600
1200
800
400
0
−13
m
C
N
Mistras lagoon
Sinis Peninsula
Tharros
0
2.5 km
D

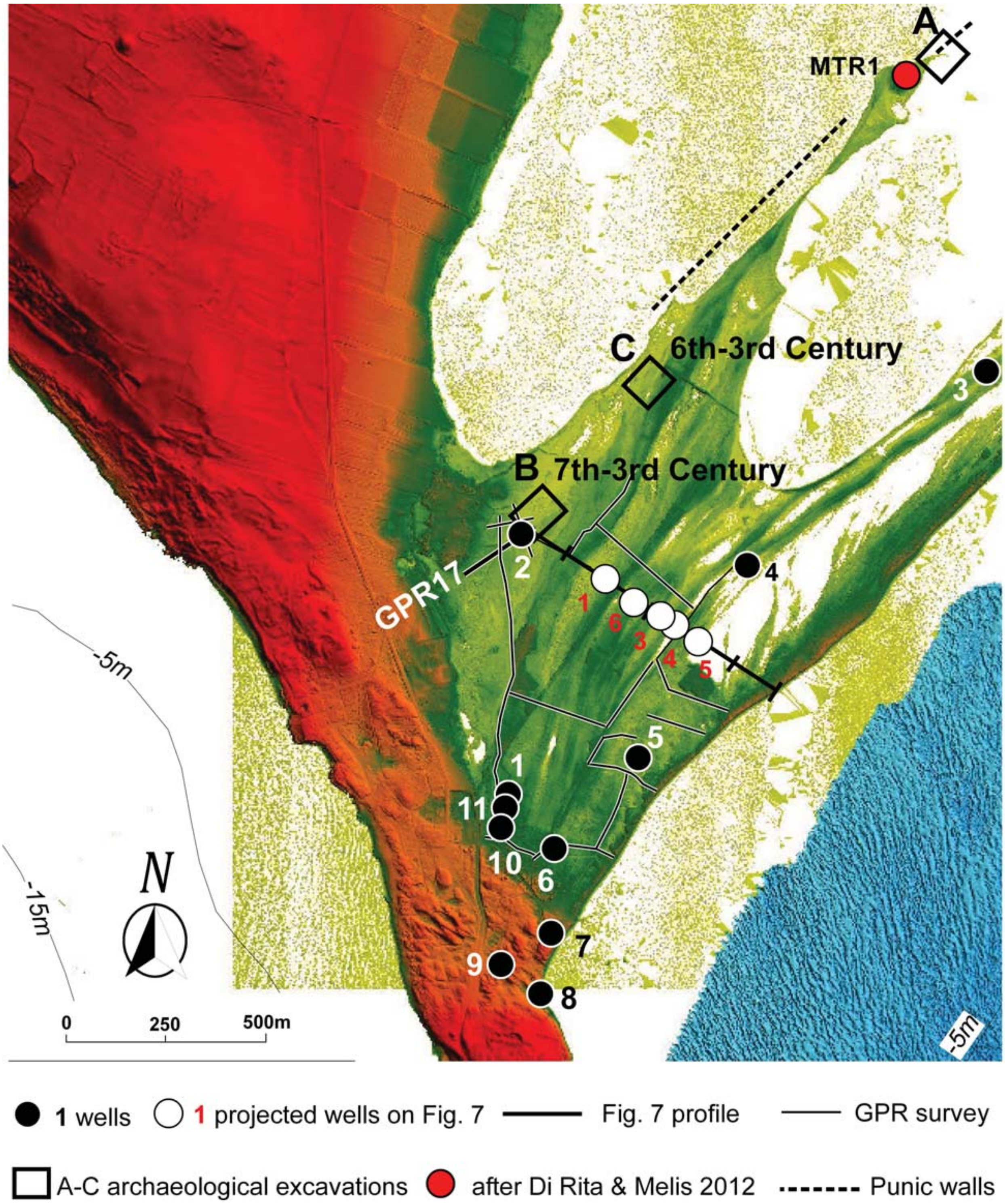
A
MTR1
C 6th-3rd Century
3
B 7th-3rd Century
2
GPR17
4
1
6
3
4
5
-5m
5
1
11
10
6
-15m
N
7
9
8
0
250
500m
-5m
1 wells
1 projected wells on Fig. 7
Fig. 7 profile
GPR survey
A-C archaeological excavations
after Di Rita & Melis 2012
Punic walls

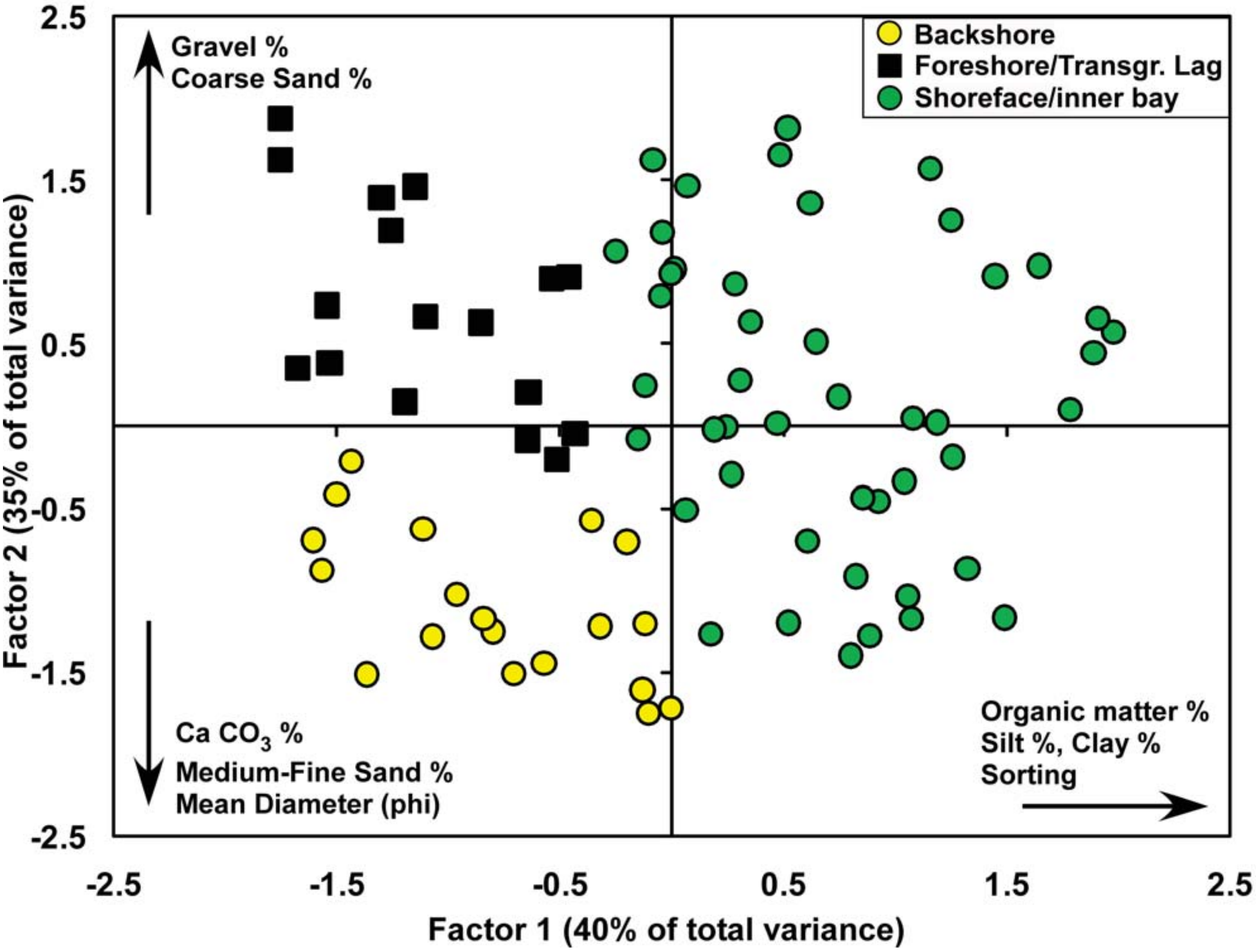

2.5
1.5
0.5
-0.5
-1.5
-2.5
-2.5
-1.5
-0.5
0.5
1.5
2.5
Factor 2 (35% of total variance)
Factor 1 (40% of total variance)
Gravel %
Coarse Sand %
Ca CO3 %
Medium-Fine Sand %
Mean Diameter (phi)
Organic matter %
Silt %, Clay %
Sorting
Backshore
Foreshore/Transgr. Lag
Shoreface/inner bay

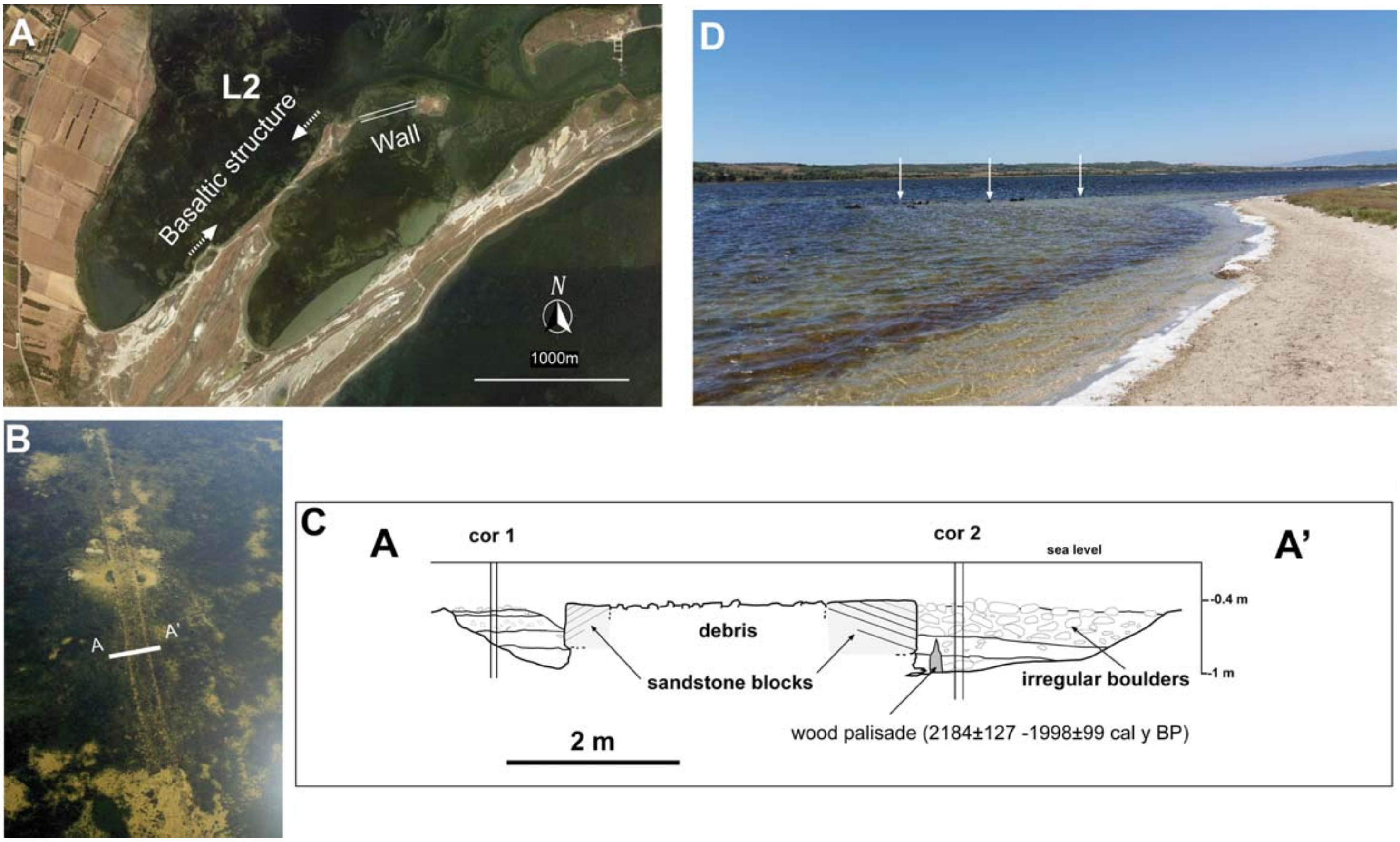
A
L2
Basaltic structure
Wall
N
1000m
D
B
A
A'
C
A
cor 1
cor 2
sea level
A'
-0.4 m
debris
sandstone blocks
irregular boulders
-1 m
wood palisade (2184±127 -1998±99 cal y BP)
2 m

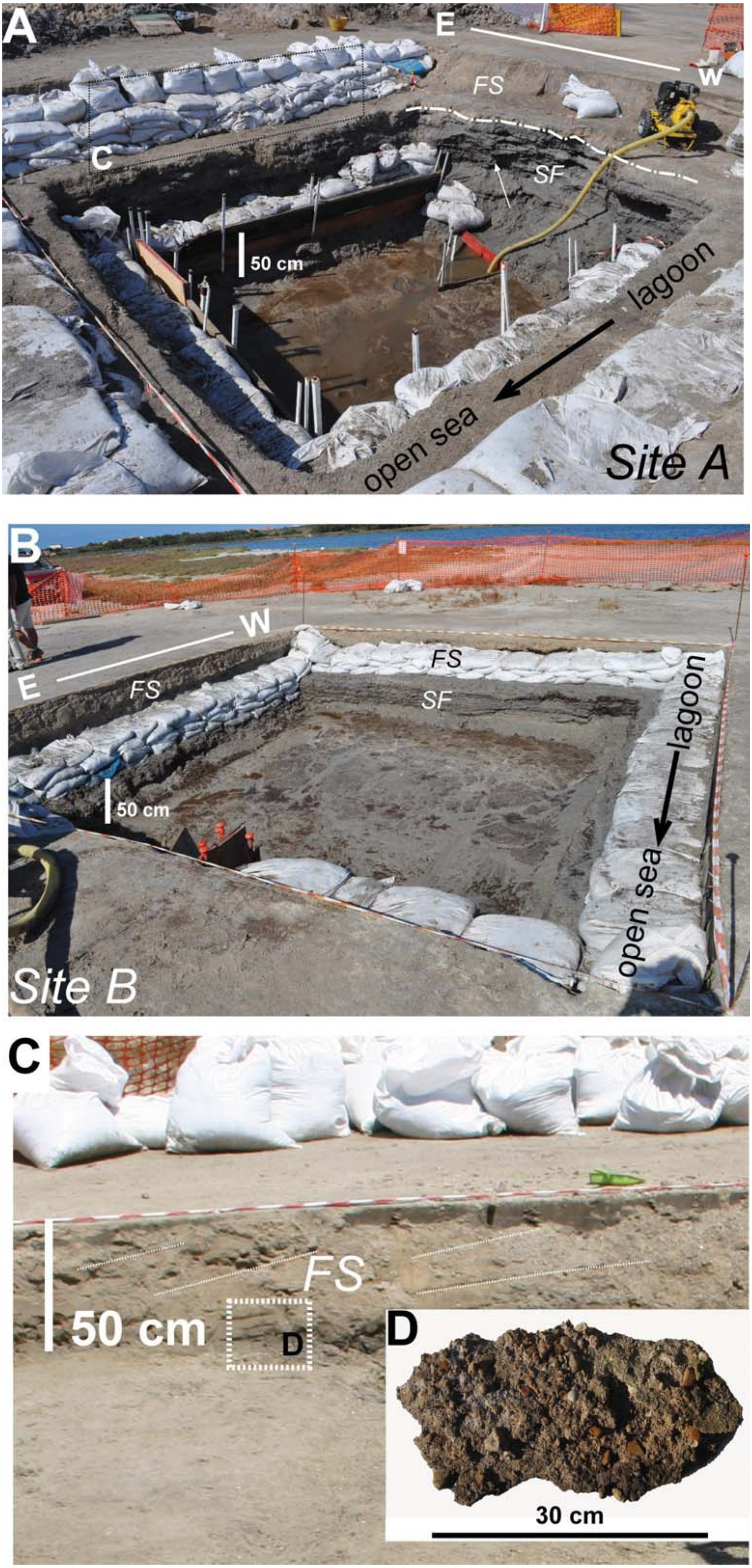

A
E
W
FS
SF
C
50 cm
lagoon
open sea
Site A
B
W
E
FS
FS
SF
lagoon
50 cm
open sea
Site B
C
FS
50 cm
D
D
30 cm

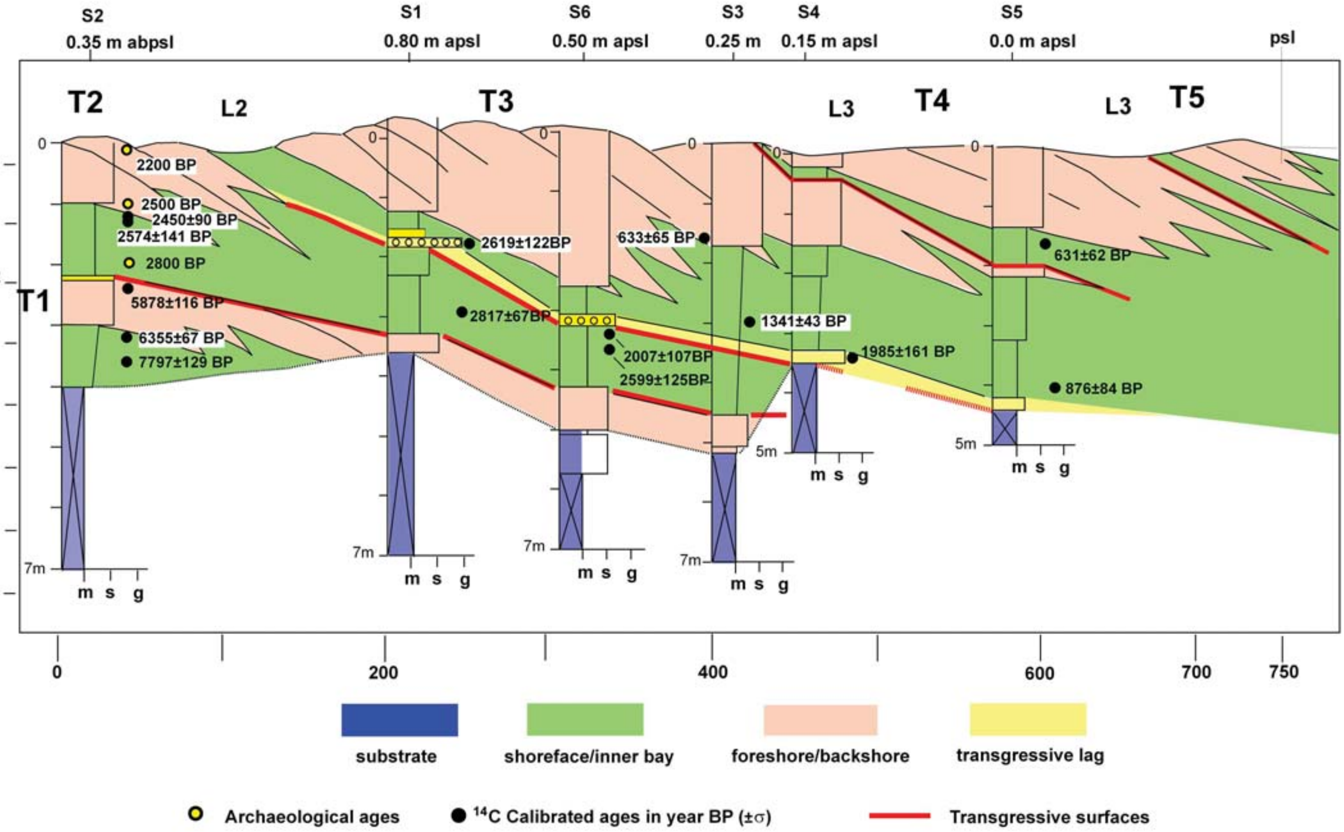

S2
0.35 m abpsl
S1
0.80 m apsl
S6
0.50 m apsl
S3
0.25 m
S4
0.15 m apsl
S5
0.0 m apsl
psl
T1
T2
L2
T3
L3
T4
L3
T5
0 msl
2
4
6
2200 BP
2500 BP
2450±90 BP
2574±141 BP
2800 BP
5878±116 BP
6355±67 BP
7797±129 BP
2619±122BP
2817±67BP
2007±107BP
2599±125BP
633±65 BP
1341±43 BP
1985±161 BP
631±62 BP
876±84 BP
7m
5m
m s g
0
200
400
600
700
750
substrate
shoreface/inner bay
foreshore/backshore
transgressive lag
Archaeological ages
^{14}C Calibrated ages in year BP (±σ)
Transgressive surfaces

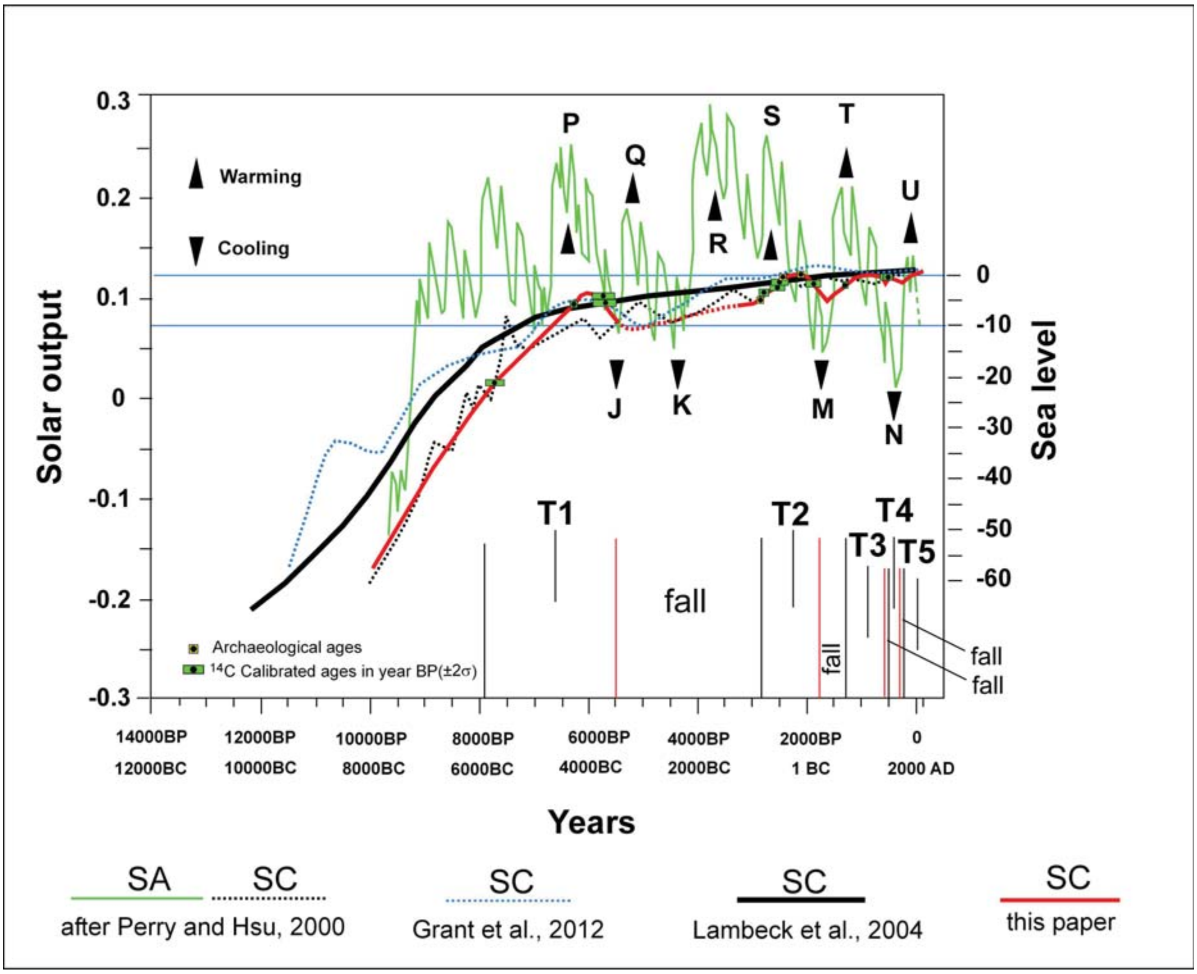

Solar output
Sea level
Warming
Cooling
P
Q
R
S
T
U
J
K
M
N
T1
T2
T3
T4
T5
fall
fall
fall
fall
Archaeological ages
^{14}C Calibrated ages in year BP(±2σ)
0.3
0.2
0.1
0
-0.1
-0.2
-0.3
0
-10
-20
-30
-40
-50
-60
14000BP 12000BC
12000BP 10000BC
10000BP 8000BC
8000BP 6000BC
6000BP 4000BC
4000BP 2000BC
2000BP 1 BC
0 2000 AD
Years
SA SC
after Perry and Hsu, 2000
SC
Grant et al., 2012
SC
Lambeck et al., 2004
SC
this paper

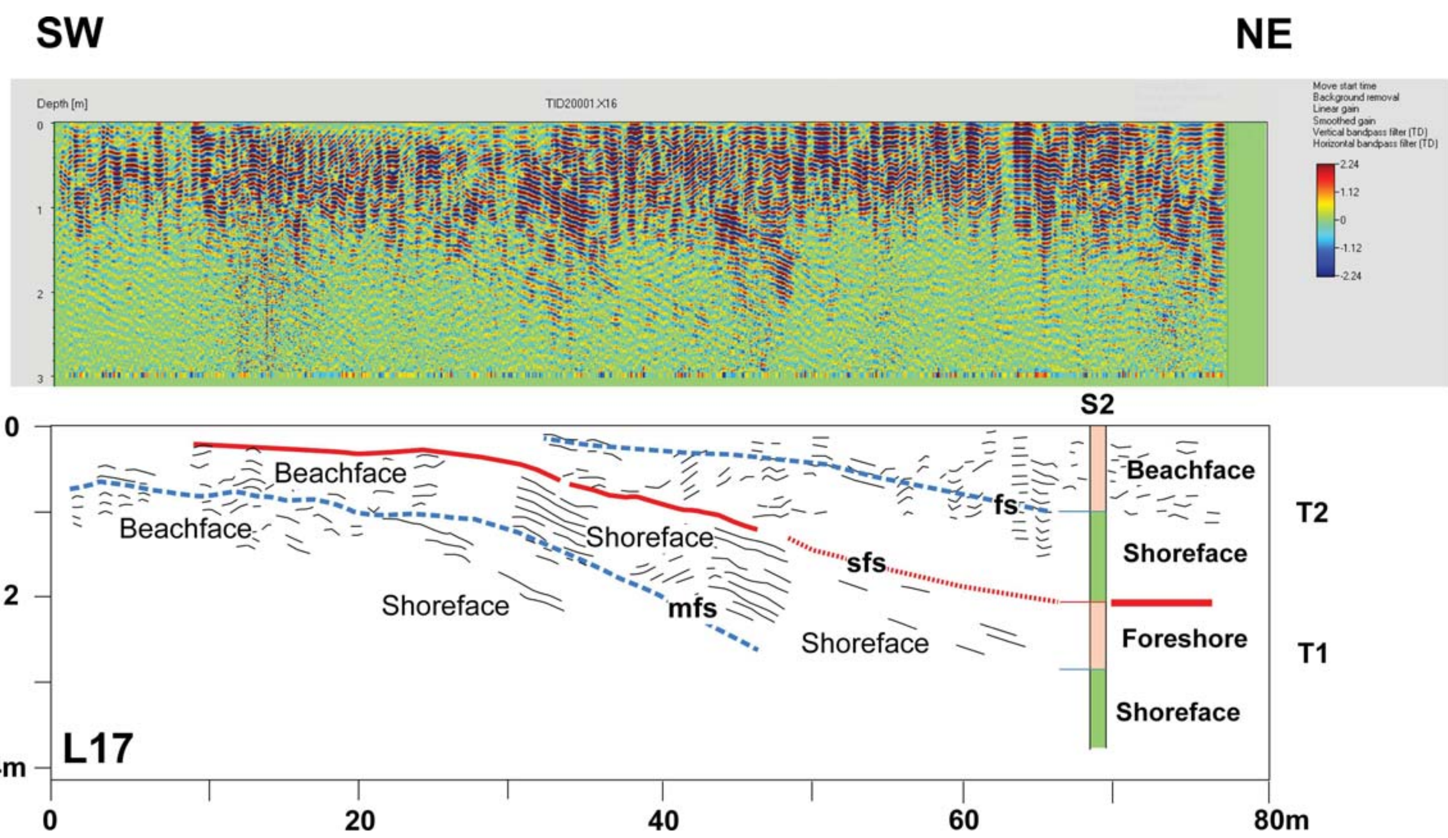

SW
NE
Depth [m]
TID20001.X16
Move start time
Background removal
Linear gain
Smoothed gain
Vertical bandpass filter (TD)
Horizontal bandpass filter (TD)
2.24
1.12
0
-1.12
-2.24
S2
Beachface
Beachface
Shoreface
Shoreface
Shoreface
fs
sfs
mfs
Beachface
Shoreface
Foreshore
Shoreface
T2
T1
L17
0
2
4m
0
20
40
60
80m

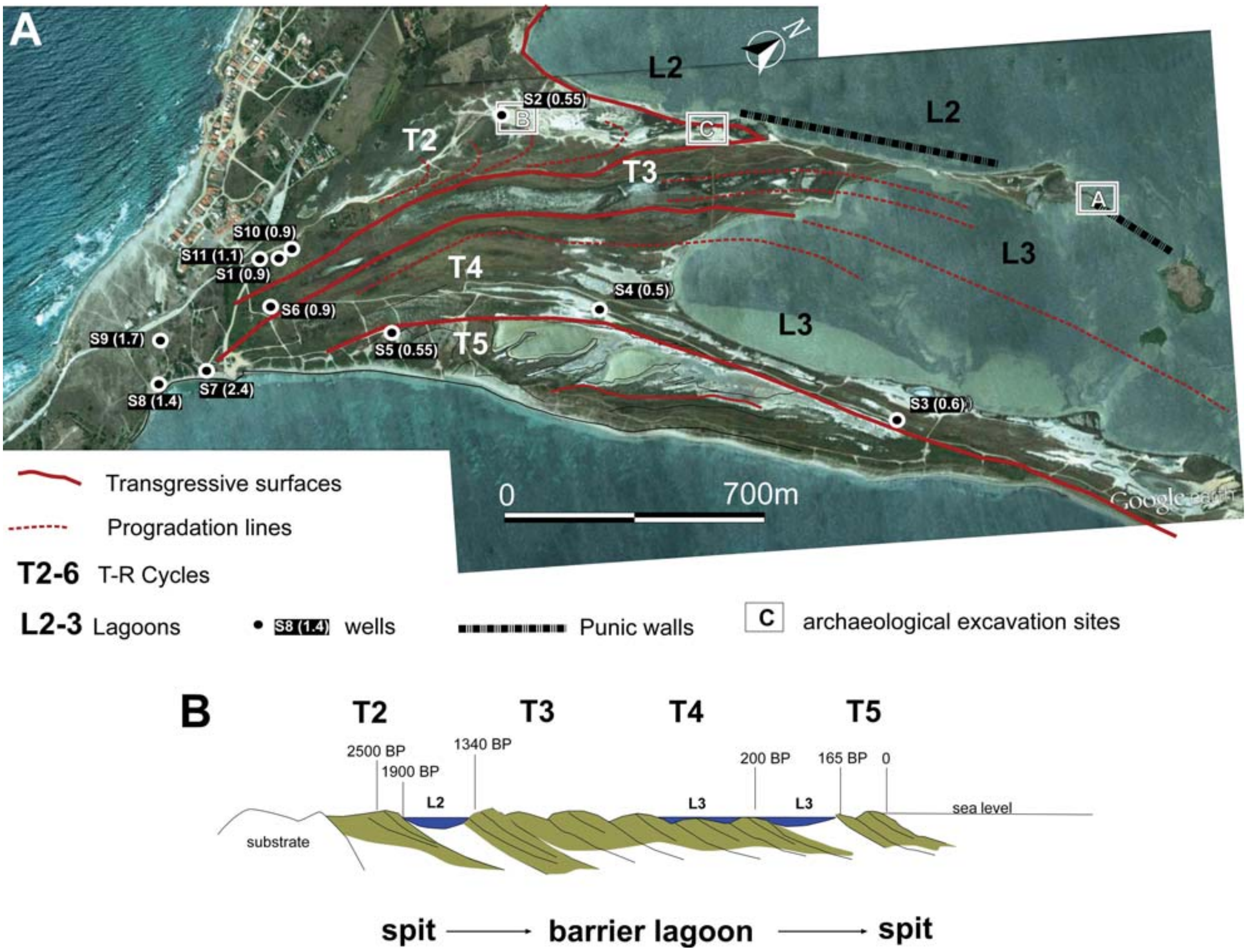
A
L2
L2
S2 (0.55)
B
C
T2
T3
A
S10 (0.9)
S11 (1.1)
S1 (0.9)
T4
S4 (0.5)
L3
S6 (0.9)
L3
S9 (1.7)
S5 (0.55)
T5
S8 (1.4)
S7 (2.4)
S3 (0.6)
0
700m
Transgressive surfaces
Progradation lines
T2-6 T-R Cycles
L2-3 Lagoons
S8 (1.4) wells
Punic walls
C archaeological excavation sites
B
T2
T3
T4
T5
2500 BP
1900 BP
1340 BP
200 BP
165 BP
0
L2
L3
L3
sea level
substrate
spit
barrier lagoon
spit

Core	Depth in core m	Sample description	Radiocarbon age Years BP	δ^{13}C (‰)	Calibration dataset	% marine	Median Calendar Age (year BP) and 2σ error	Minimum-Maximum calendar age year BP (2σ)
S1	1.90	Bone Fragment	2558±23	-23±1	Mixed Marine NoHem	8%	2619±122	2741-2497
	2.50	Posidonia Fibers	2806±37	-19±1	Mixed Marine NoHem	24%	2817±67	2884-2750
S2	2.24	Posidonia Fibers	5243±35	-20±2	Mixed Marine NoHem	20%	5878±116	5993-5762
	3.23	Shell	5737±32	-15±2	Mixed Marine NoHem	40%	6355±67	6421-6288
	3.73	Shell	7059±56	-18±1	Mixed Marine NoHem	28%	7797±129	7925-7668
S3	1.57	Posidonia Fibers	883±22	-15±2	Mixed Marine NoHem	40%	633±65	699-568
	2.25	Posidonia Fibers	1559±21	-18±1	Mixed Marine NoHem	28%	1341±43	1383-1298
S4	3.40	Shell	2019±69	-48±1	Intcal13		1985±161	2147-1824
S5	1.22	Posidonia Fibers	716±27	-27±1	Intcal13	44%	631±62	693-569
	4.01	Posidonia Fibers	1160±35	-14±2	Mixed Marine NoHem		876±84	960-792
S6	3.05	Bone Fragment	2039±36	-26±2	Intcal13	44%	2007±107	2113-1900
	3.39	Posidonia Fibers	2671±29	-14±2	Mixed Marine NoHem		2599±125	2725-2474
S7	3.49	Posidonia Fibers	781±26	-7±1	Mixed Marine NoHem	72%	486±55	541-431
	6.39	Posidonia Fibers	5260±55	-7±2	Mixed Marine NoHem	72%	5723±138	5861-5585
S10	1.50	Posidonia Fibers	2510±26	-25±2	Intcal13	44%	2614±124	2738-2490
	2.37	Posidonia Fibers	2829±35	-14±1	Mixed Marine NoHem		2778±62	2850-2726
C1	1.1	Pinecone	2210±57	-18±1	Mixed Marine NoHem	28%	2115±185	2300-1930
C2	0.9	Wood fragment	2169±39	-43±1	Intcal13	48%	2184±127	2311-2057
C3	1.1	Wood fragment	2215±25	-18±1	Mixed Marine NoHem		1998±99	2098-1899
US21-SE	1.0	Seed	2446±23	-19±1	Intacl13		2528±170	2699-2358
US26-SE	1.5	Seed	2470±23	-20±1	Intacl13		2537±172	2710-2365
US35-SE	2.0	Seed	2448±24	-34±3	Intacl13		2529±170	2700-2359

Environment of deposition		$CaCO_3$ %	Organic Matter %	Gravel %	Coarse Sand %	Medium-Fine sand %	Sortable Silt (11-63 µm) %	Non Sortable (<11µm) %	Mean Diameter phi	Sorting
Backshore	Mean	61.2	2.6	1.1	15.1	74.8	7.7	1.2	2.3	1.4
	sd	8.6	1.9	1.9	8.6	6.7	4.4	0.9	0.4	0.2
Foreshore Transgressive lag	Mean	45.3	1.5	12.9	43.5	42.0	4.2	1.0	1.3	1.6
	sd	13.9	1.0	11.5	18.4	18.4	2.7	0.8	0.7	0.4
Shoreface	Mean	49.6	8.5	8.3	29.7	41.1	15.3	5.6	2.2	2.3
	sd	16.7	11.0	13.9	11.5	16.7	6.9	3.6	0.8	0.4

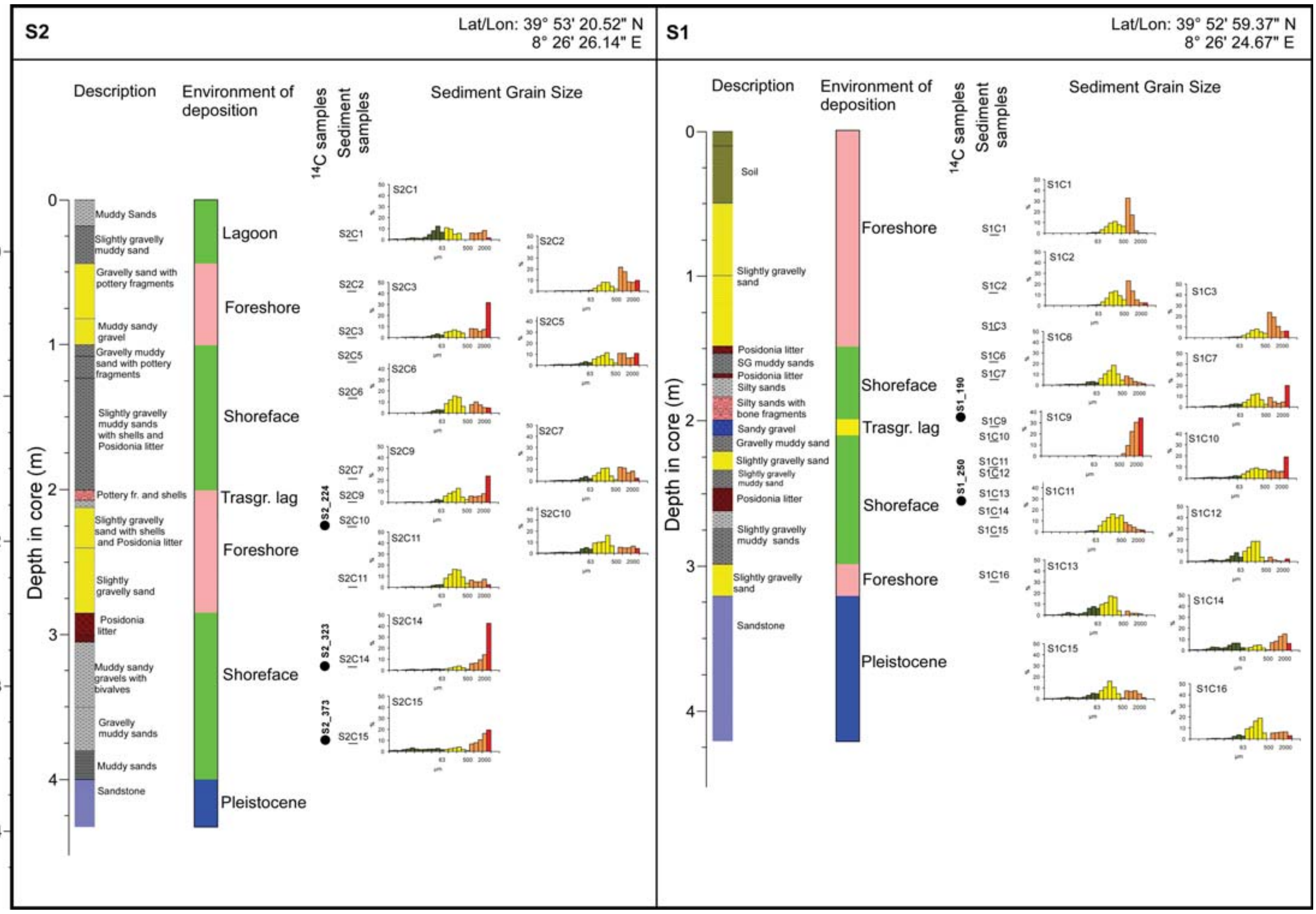

S2
Lat/Lon: 39° 53' 20.52" N
8° 26' 26.14" E
Description
Environment of deposition
14C samples
Sediment samples
Sediment Grain Size
Depth below present sea level (m)
Depth in core (m)
Muddy Sands
Slightly gravelly muddy sand
Gravelly sand with pottery fragments
Muddy sandy gravel
Gravelly muddy sand with pottery fragments
Slightly gravelly muddy sands with shells and Posidonia litter
Pottery fr. and shells
Slightly gravelly sand with shells and Posidonia litter
Slightly gravelly sand
Posidonia litter
Muddy sandy gravels with bivalves
Gravelly muddy sands
Muddy sands
Sandstone
Lagoon
Foreshore
Shoreface
Trasgr. lag
Foreshore
Shoreface
Pleistocene
S2_224
S2_323
S2_373
S2C1
S2C2
S2C3
S2C5
S2C6
S2C7
S2C9
S2C10
S2C11
S2C14
S2C15
S1
Lat/Lon: 39° 52' 59.37" N
8° 26' 24.67" E
Description
Environment of deposition
14C samples
Sediment samples
Sediment Grain Size
Depth in core (m)
Soil
Slightly gravelly sand
Posidonia litter
SG muddy sands
Posidonia litter
Silty sands
Silty sands with bone fragments
Sandy gravel
Gravelly muddy sand
Slightly gravelly sand
Slightly gravelly muddy sand
Posidonia litter
Slightly gravelly muddy sands
Slightly gravelly sand
Sandstone
Foreshore
Shoreface
Trasgr. lag
Shoreface
Foreshore
Pleistocene
S1_190
S1_250
S1C1
S1C2
S1C3
S1C6
S1C7
S1C9
S1C10
S1C11
S1C12
S1C13
S1C14
S1C15
S1C16

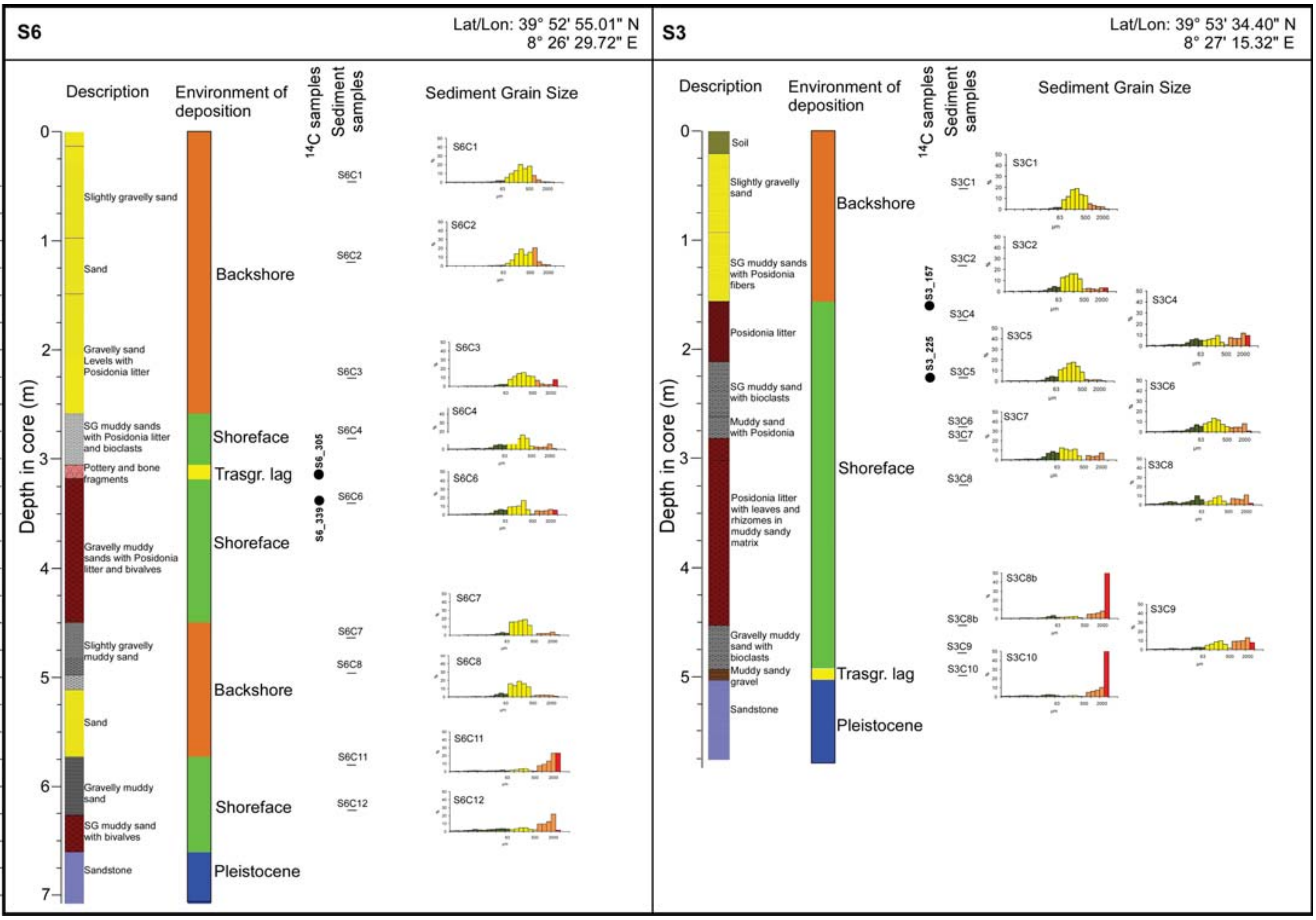

S6
Lat/Lon: 39° 52' 55.01" N
8° 26' 29.72" E
Description
Environment of deposition
14C samples
Sediment samples
Sediment Grain Size
Depth below present sea level (m)
Depth in core (m)
Slightly gravelly sand
Sand
Gravelly sand Levels with Posidonia litter
SG muddy sands with Posidonia litter and bioclasts
Pottery and bone fragments
Gravelly muddy sands with Posidonia litter and bivalves
Slightly gravelly muddy sand
Sand
Gravelly muddy sand
SG muddy sand with bivalves
Sandstone
Backshore
Shoreface
Trasgr. lag
Shoreface
Backshore
Shoreface
Pleistocene
S6_305
S6_339
S6C1
S6C2
S6C3
S6C4
S6C6
S6C7
S6C8
S6C11
S6C12
S3
Lat/Lon: 39° 53' 34.40" N
8° 27' 15.32" E
Description
Environment of deposition
14C samples
Sediment samples
Sediment Grain Size
Depth in core (m)
Soil
Slightly gravelly sand
SG muddy sands with Posidonia fibers
Posidonia litter
SG muddy sand with bioclasts
Muddy sand with Posidonia
Posidonia litter with leaves and rhizomes in muddy sandy matrix
Gravelly muddy sand with bioclasts
Muddy sandy gravel
Sandstone
Backshore
Shoreface
Trasgr. lag
Pleistocene
S3_157
S3_225
S3C1
S3C2
S3C4
S3C5
S3C6
S3C7
S3C8
S3C8b
S3C9
S3C10

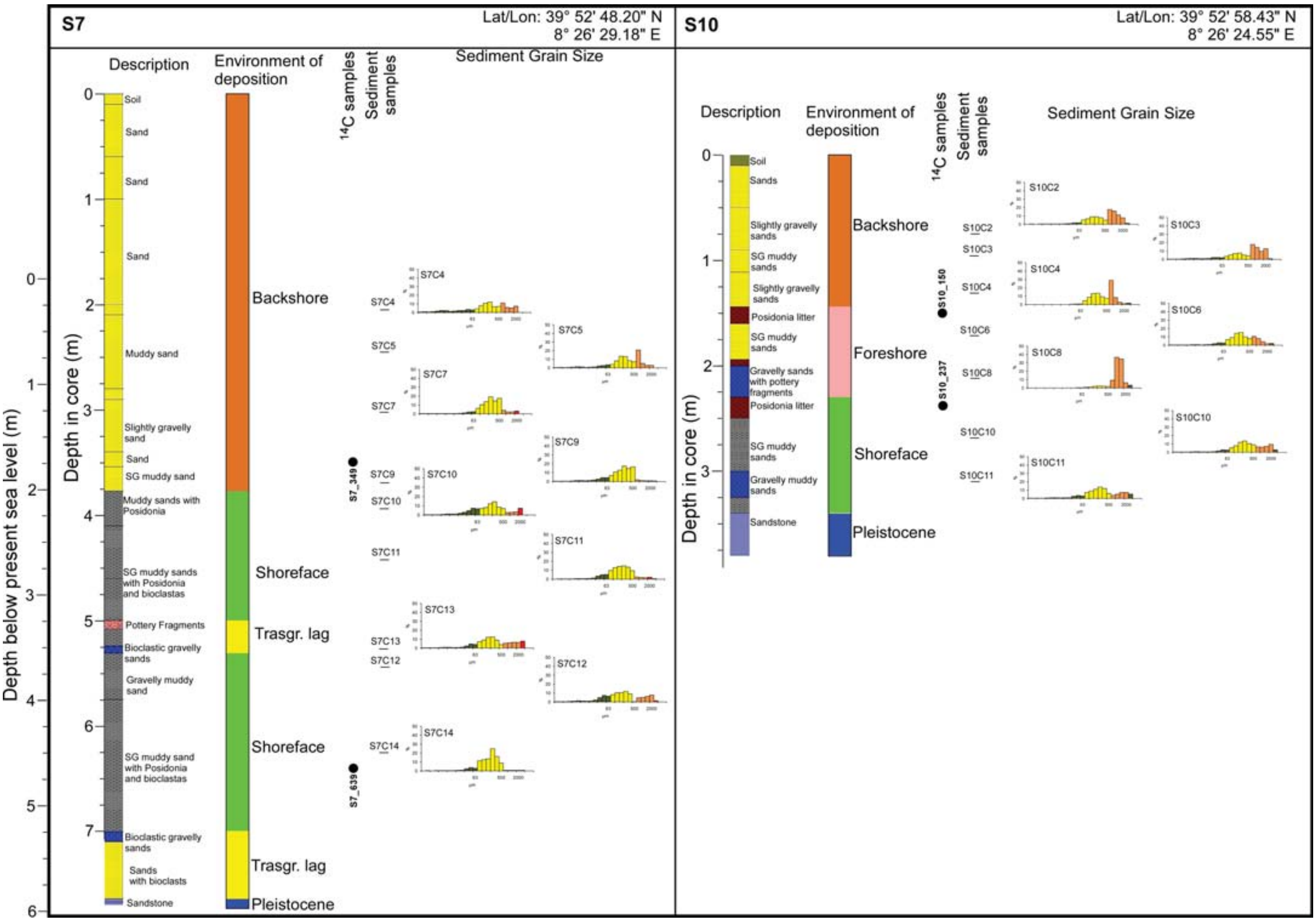

S7
Lat/Lon: 39° 52' 48.20" N
8° 26' 29.18" E
Description
Environment of deposition
14C samples
Sediment samples
Sediment Grain Size
Depth in core (m)
Depth below present sea level (m)
Soil
Sand
Muddy sand
Slightly gravelly sand
SG muddy sand
Muddy sands with Posidonia
SG muddy sands with Posidonia and bioclastas
Pottery Fragments
Bioclastic gravelly sands
Gravelly muddy sand
SG muddy sand with Posidonia and bioclastas
Sands with bioclasts
Sandstone
Backshore
Shoreface
Trasgr. lag
Pleistocene
S7_349
S7_639
S7C4
S7C5
S7C7
S7C9
S7C10
S7C11
S7C13
S7C12
S7C14
S10
Lat/Lon: 39° 52' 58.43" N
8° 26' 24.55" E
Sands
Slightly gravelly sands
SG muddy sands
Posidonia litter
Gravelly sands with pottery fragments
Gravelly muddy sands
Foreshore
S10_150
S10_237
S10C2
S10C3
S10C4
S10C6
S10C8
S10C10
S10C11

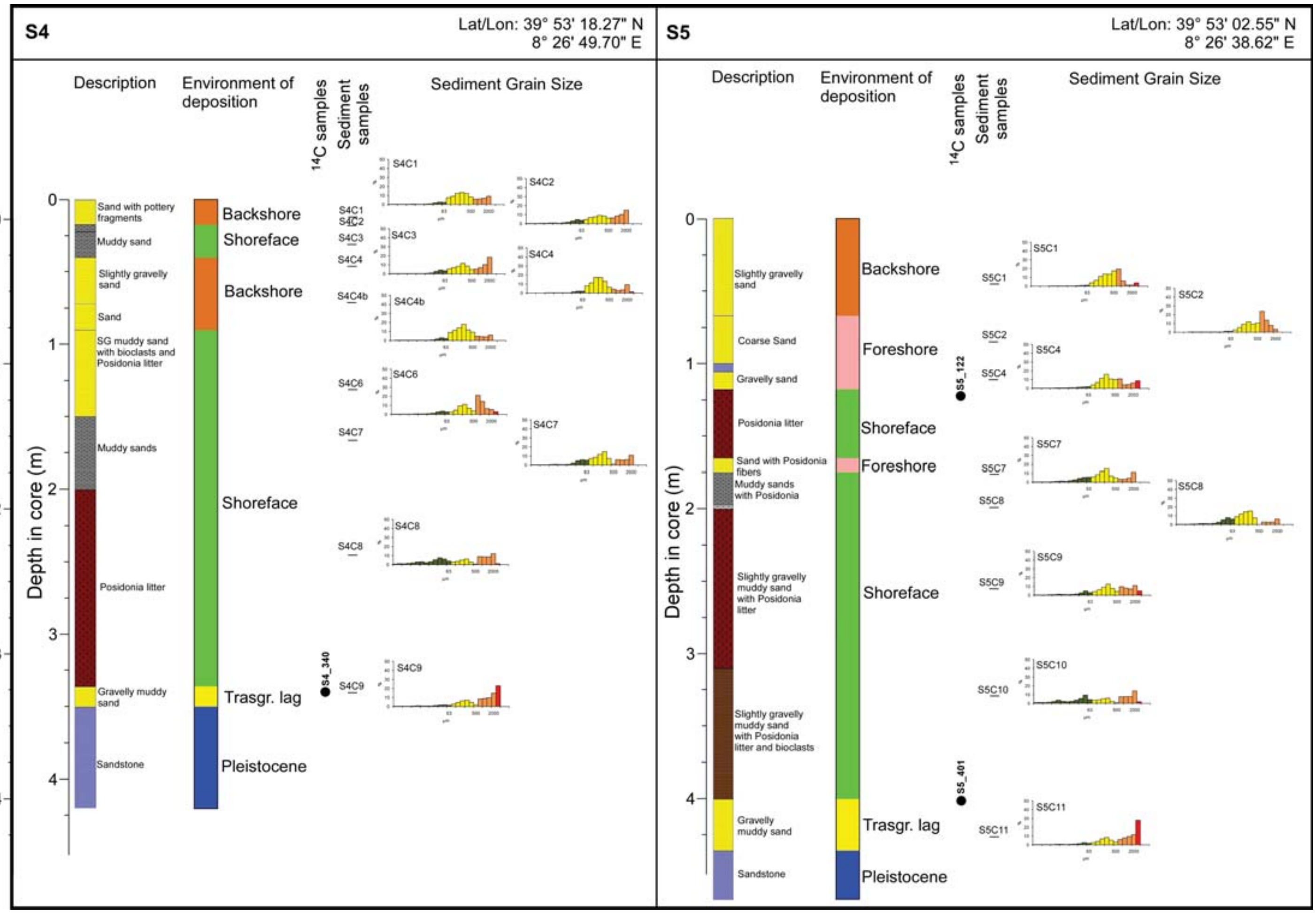
S4
Lat/Lon: 39° 53' 18.27" N
8° 26' 49.70" E
Description
Environment of deposition
14C samples
Sediment samples
Sediment Grain Size
Depth below present sea level (m)
Depth in core (m)
Sand with pottery fragments
Muddy sand
Slightly gravelly sand
Sand
SG muddy sand with bioclasts and Posidonia litter
Muddy sands
Posidonia litter
Gravelly muddy sand
Sandstone
Backshore
Shoreface
Backshore
Shoreface
Trasgr. lag
Pleistocene
S4_340
S4C1
S4C2
S4C3
S4C4
S4C4b
S4C6
S4C7
S4C8
S4C9
S5
Lat/Lon: 39° 53' 02.55" N
8° 26' 38.62" E
Description
Environment of deposition
14C samples
Sediment samples
Sediment Grain Size
Depth in core (m)
Slightly gravelly sand
Coarse Sand
Gravelly sand
Posidonia litter
Sand with Posidonia fibers
Muddy sands with Posidonia
Slightly gravelly muddy sand with Posidonia litter
Slightly gravelly muddy sand with Posidonia litter and bioclasts
Gravelly muddy sand
Sandstone
Backshore
Foreshore
Shoreface
Foreshore
Shoreface
Trasgr. lag
Pleistocene
S5_122
S5_401
S5C1
S5C2
S5C4
S5C7
S5C8
S5C9
S5C10
S5C11